

The determination of turbulent structures  
in the atmospheric surface layer

BIBLIOTHEEK L.H.  
0 5 DEC. 1984  
ONTV. TIJDSCHR. ADM.

CENTRALE LANDBOUWCATALOGUS



0000 0060 0623

40951

**Promotor:** dr. ir. L. Wartena,  
hoogleraar in de landbouweerkunde en  
omgevingsnatuurkunde

**Co-promotor:** dr. ir. A. C. M. Beljaars,  
wetenschappelijk medewerker bij de  
afdeling Fysische Meteorologie van het  
Koninklijk Nederlands Meteorologisch  
Instituut te De Bilt

J. L. J. Schols

# The determination of turbulent structures in the atmospheric surface layer

## Proefschrift

ter verkrijging van de graad van  
doctor in de landbouwwetenschappen,  
op gezag van de rector magnificus,  
dr. C. C. Oosterlee,  
in het openbaar te verdedigen  
op vrijdag 21 december 1984  
des namiddags te vier uur in de aula  
van de Landbouwhogeschool te Wageningen.

## STELLINGEN

### I

Er bestaat nog geen objectieve methode voor de detectie van turbulente structuren.

### II

Het begrip locale isotropie impliceert niet dat de directe koppeling tussen grootschalige en kleinschalige bewegingen gering is.

### III

Individuele turbulente structuren in de oppervlaktegrenslaag van de atmosfeer hebben een relatief korte levensduur, terwijl het integrale effect van hun aanwezigheid een grotere tijdschaal heeft.

### IV

De koppeling tussen de turbulente transporten boven en binnen gewassen komt hoofdzakelijk tot stand via de turbulente statische drukfluctuaties.

### V

Het zou de bestrijding van winderosie van grond en windschade aan gewassen in Afrika ten goede komen als kwantitatief onderzoek aan traditionele methoden zou worden gedaan.

### VI

Boeren en tuinders kunnen beter gebruik maken van de landbouwweerberichtgeving, indien het onderwijs in de meteorologie op land- en tuinbouwscholen wordt uitgebreid.

### VII

Het weer is een turbulent gebeuren.

### VIII

Het begrip weersverwachting impliceert dat we van het weer nog iets te verwachten hebben.

### IX

De bruikbaarheid van weersverwachtingen kan worden verbeterd door de gebruiker vooraf te informeren over de mate van betrouwbaarheid van die verwachtingen.

X

De huidige wetenschapsbeoefening zou sterk gebaat zijn met een modern management.

XI

De rol die serendipiteit speelt bij wetenschappelijke vooruitgang en ontdekkingen wordt veelal onderschat.

XII

Indien de huidige trend in het regeringsbeleid ten aanzien van de kunsten zich voortzet zal dat beleid binnen korte tijd weer gereduceerd zijn tot haar oorspronkelijke functie: Monumentenzorg.

XIII

De mens is wat hij van zich zelf maakt.

Jean-Paul Sartre.

XIV

De Universele Verklaring van de Rechten van de Mens van 1948 is verbazend Westers en derhalve niet algemeen.

XV

Het tijdperk van de eenvoudige, elegante fysica ligt achter ons.

XVI

De anti-misbruikwetgeving is een goed voorbeeld van legislatieve onmacht.

XVII

Veel stellingen zijn teleurstellingen.

J.L.J. Schols

The determination of turbulent structures in the atmospheric surface layer

Wageningen, 21 December 1984

aan mijn ouders

## Preface

This thesis contains the results of research which lasted four years. The character of the study is in part basic, as indicated by support received from the Working Group on Meteorology and Physical Oceanography (MFO) and financial aid from the Netherlands Organization for the Advancement of Pure Research (ZWO). That the results of the present investigations also have many applications, however, is indicated by support from the Department of Physics and Meteorology of the Agricultural University of Wageningen (LHW).

I am indebted to Bert Wartena, whose effort was central in obtaining financial support for the present study. He also gave me the opportunity to work according to my own ideas with a large amount of freedom. His comments during the course of this research have been invaluable and have had a strong influence on my viewpoints and deepened my insights into the subject.

Part of the present research was a field experiment, carried out at one of the meteorological sites at the Minderhoudhoeve near Swifterbant in the Oostelijk-Flevoland polder. I am very grateful to Mr. E. Kloosterman and Mr. Tj. van der Wal and their staff for the possibility of carrying out this research in their grasslands. The enthusiasm and will power with which the members of the department assisted me during the field measurements were an asset to the working atmosphere. In particular, I would like to acknowledge the co-operation of Anton Jansen, Peter Jansen, Dick Welgraven and Bart Verhaaf.

Knowledge and experience are two boundary conditions necessary to carry out an outdoor experiment. These two prerequisites are present in the mechanics and electronics workshops. The members of these workshops furnished the instrumentation and data-acquisition systems, which were necessary for obtaining the high quality measurements. For this reason I am grateful to Kees van Asselt, Geerten Lenters, Teun Jansen and Willy Hillen.

Jon Krom developed the very efficient programs for running the data-acquisition procedures and therefore I am also much obliged to him.

The processing of the measurement data has been done by a PDP11/34 computer at the laboratory. The computersystem operates under the supervision of Wim Driessen, who also designed an important part of the software for the data-acquisition system. Dimitri van den Akker was responsible for the writing of the software programs, which were necessary to process the data. Therefore, I thank these members of the Section of Measurement, Control and Systems Engineering.

The outdoor experiments could only be done under very restricted weather conditions. The weather forecasts were provided by John Bernard and Wim Vaags. Their support is greatly acknowledged.

I have received additional support from people outside of the department. Part of the data, on which this study is based, was made available by the Royal Netherlands Meteorological Institute (KNMI). I would like to acknowledge Ad Driedonks and Anton Beljaars for their efforts in providing the data. These data have been processed by the Burroughs 7700 computer at the Computer Centre of the Technical University of Eindhoven (RC-THE). Hans Vugts lent us the inclinometers, which formed an essential component of our measuring equipment. Infrared line scanning (IRLS) pictures of the measuring site at the Minderhoudhoeve have been supplied by Eurosense b.v. These remote sensing images have been processed by Mr. J. Clevers of the Department of Land Surveying and Remote Sensing of the LHW. Students of the Technical University of Eindhoven (THE) and the College of Advanced Technology (HTS) of Eindhoven have made very useful contributions to this research during their terms of probation. In this respect, I am grateful to Louis Stevens, Erik Keune, Peter van Engelen, Rob Petterson, Alex van den Berk, Rob Boesten, Frank van Galen and Jef Hopmans.

Financial affairs have always been perfectly arranged by Bas Lammers and Gerfriede Hoekendijk - de Wal. Travelling expenses for the journey between the laboratory and the measuring site have been restituted by the Fund for Agricultural Research (LEB fonds).

The journal articles have been skilfully reviewed by my colleagues Leo Kroon, John Bernard and Adrie Jacobs. An American friend of mine, Lee Ann Weeks, has given useful comments on the linguistic usage throughout the thesis. The writing of this thesis also has been influenced by useful discussions with my colleagues Cor Nieuwvelt, Rob Blokland and Hans Bessem of the Laboratory for Fluid Dynamics and Heat Transfer of the Department of Applied Physics of the THE.

It is worth mentioning that Paul van Espelo made the drawings and prepared the illustrations in an outstanding manner. The final version of this thesis was most accurately typed by Lenny Weldring. The printing of this booklet was done by the graphic office Ponsen & Looijen in Wageningen.

The members of the secretariate have always taken care of administrative matters and have furnished overhead facilities. I want to express my gratitude to Coby v.d. Pol - van Lienden, Corry Pitlo, Marja van Steenbergen and Gré Heitkönig.

I want to thank Dane Bičanić for being a pleasant car-mate during the commuting between Wageningen and our residence Nijmegen.

Finally, I am obliged to all the people who directly or indirectly have collaborated with me and whose names I have somehow managed to not mention.

# Contents

## Notation

### I. General introduction

1. Background of the present study	I.1
2. Purpose of the present study	I.2
3. Review of recent research	I.3
4. Organization of the thesis	I.4

### II. The detection and measurement of turbulent structures in the atmospheric surface layer

Abstract	II.1
1. Introduction	II.2
2. The present investigation	II.3
3. Results of the use of the VITA detection technique to measure turbulent structures in the atmospheric surface layer	II.8
4. Conclusions	II.23

### III. Characteristics of turbulent structures in the unstable atmospheric surface layer

Abstract	III.1
1. Introduction	III.2
2. Experimental details	III.2
2.1. Site and instrumentation	III.2
2.2. Data acquisition and processing	III.6
2.3. Selection and description of the data	III.7
3. Experimental results	III.10
3.1. Contribution of turbulent structures to turbulent vertical transports	III.12
3.2. Temporal behavior	III.13
3.2.1. Translation speed	III.13
3.2.2. Lifetime	III.17

3.3. Spatial distribution	III.22
3.3.1. Inclination angle	III.22
3.3.2. Horizontal distribution	III.22
4. Formation mechanism	III.24
5. Conclusions	III.26
IV. A dynamical description of the turbulent structures in the near neutral atmospheric surface layer: The role of static pressure fluctuations	
Abstract	IV.1
1. Introduction	IV.2
2. Pressure instrumentation	IV.2
3. Dynamics of turbulent structures	IV.5
3.1. Scale characteristics	IV.6
3.2. Static pressure-velocity (gradient) relationships	IV.9
4. The role of static pressure fluctuations in the mechanism of the origin and development of the turbulent structures	IV.12
5. Conclusions	IV.13
V. Discussion	
Appendix A. Horizontal wind speed averaged over the depth of the ASL	
Appendix B. Convection cells in the unstable ASL	
Appendix C. Stagnation pressure	
Appendix D. Turbulent kinetic energy budget	
Appendix E. Pressure gradient force	

Summary

Samenvatting

References

Curriculum vitae

## Notation

### Latin symbols

A	numerical factor ( $\lambda = 0.026 \text{ ms}^{-2} \text{K}^{-1}$ )
B	numerical factor ( $\lambda = 260 \text{ m}^{-1} \text{s}^2 \text{K}$ )
C	numerical factor ( $\lambda = 3400 \text{ m}^{-2} \text{s}^2 \text{K}$ )
Coh	coherence function
$\text{Co}_{ij}$	co-spectrum between two turbulent signals
d	detection signal
f	frequency in Hz or turbulent quantity
$f_s$	sampling rate in Hz
Fm	modified Froud number
g	acceleration due to gravity ( $= 9.81 \text{ ms}^{-2}$ )
G	power spectral density function
h	height in m
j	imaginary unit ( $= \sqrt{-1}$ )
k	von Kármán constant ( $= 0.4$ ) or threshold level
L	Obukhov length ( $= -u_*^3 \bar{T} / (k.g. \overline{w'T'})$ ) in m
l	length in m
N	number of samples
n	number of detected turbulent structures
p	static pressure in $\text{Nm}^{-2}$ or percentage
$q'^2$	specific turbulent kinetic energy in $\text{m}^2 \text{s}^{-2}$
Q	quadrature spectrum
r	mixing ratio
Ra	Rayleigh number
t	time in s
T	Temperature in °C or K
$T_*$	temperature scale in ASL ( $= -\overline{w'T'} / u_*$ ) in K or °C
$U_c$	translation speed in $\text{ms}^{-1}$
$U_p$	phase speed in $\text{ms}^{-1}$
U,V,W	alongwind, crosswind, vertical components of wind velocity in $\text{ms}^{-1}$
$u_*$	surface friction velocity ( $= (-\overline{u'w'})^{1/2}$ ) in $\text{ms}^{-1}$
x,y,z	alongwind, crosswind, vertical coordinate directions in m

$z_0$  surface roughness length in m  
 $z_i$  lowest inversion height in m

#### Greek symbols

$\gamma$  time fraction  
 $\Delta$  Laplace operator ( $= \nabla^2$ ) in  $m^{-2}$  or increment  
 $\epsilon$  dissipation rate of specific turbulent kinetic energy  
 in  $m^2 s^{-3}$   
 $\theta$  angle  
 $\lambda$  wavelength in m  
 $\pi$  3.141 .....  
 $\rho$  air density ( $\approx 1.2 \text{ kgm}^{-3}$ )  
 $\sigma_f$  standard deviation of turbulent fluctuations  
 $\tau$  timescale in s  
 $\phi$  phase angle or  
 azimuth angle  
 $\phi_H$  dimensionless temperature gradient  
 ( $= (kz/T_*) \partial \bar{T} / \partial z$ )  
 $\phi_m$  dimensionless wind shear  
 ( $= (kz/u_*) \partial \bar{U} / \partial z$ )

#### Special notation

$E [ ]$  ensemble average  
 $\ln$  natural logarithm  
 $\nabla$  gradient operator in  $m^{-1}$   
 overbar time average over a time which is long compared to the  
 largest turbulence timescale and short compared to the  
 timescale of the mesoscale variations of the flow field  
 prime turbulent fluctuation  
 underbar vector quantity  
 $\text{var}( )$  short-time variance

# I. General introduction

Knowledge of the structure of turbulence in the planetary boundary layer (PBL) in the daytime leads to many applications in a variety of fields such as aviation, air pollution dispersion, agriculture, wind engineering, wind energy and urban planning. The exchange of mass, momentum and heat between the earth's surface and the atmosphere is mainly governed by the turbulent transport in the PBL. The turbulent transport mechanism has a marked effect on atmospheric motions. In order to reach the objectives of accurate long range numerical forecasts it is necessary to be able to model the turbulent exchange effectively. Because of the low resolution of numerical models the turbulent exchanges must be expressed in terms of large scale parameters. Another important application of the knowledge of the structure of turbulence in the PBL is in the field of transmissions. In the propagation of electromagnetic radiation through the atmosphere the largest changes in refractive index, which account for a significant fraction of signal degradation, will occur at the temperature and humidity discontinuities at the boundaries of turbulent structures. Turbulent structures are defined as spatially coherent, organized flow motions. 'Organized' means that characteristic patterns, observed at a point in space, occur almost simultaneously in more than one turbulence signal and are repeated periodically.

## 1. Background of the present study

Turbulence is non-predictive and is still one of the major unsolved problems of classical physics. This type of fluid motion is described by Newton's second law of motion and is basically deterministic. However, strong non-linear interactions between the various scales of motion cause the turbulent field to appear as a chaotic motion.

From an engineering point of view one is generally only interested in the mean quantities of the turbulent flow field, such as

mean profiles of velocity, temperature and humidity, and coefficients of heat transfer and surface friction. A large part of the study of turbulence is concerned with the development of models which are used to compute these averages. The approach of the turbulence problem is a statistical one.

Long time averages, over e.g. half an hour, rather hide than reveal the physics of a chaotic motion. By performing a conventional averaging process on the flow equations following Reynolds' method (Reynolds, 1895) certain information is lost that is essential to the understanding of the turbulence mechanism itself. The statistical processing of turbulence data has been renewed by the discovery of the intermittent nature of laboratory shear flows. In this respect the concept of conditional averaging has been introduced in order to study turbulent structures. Conditional averaging means that ensemble averages of the turbulent signals are computed around the time that a turbulent structure has been detected.

Two decades have passed since the earliest observations of organized structure in turbulence. Yet progress in incorporating the knowledge of this structure into practical engineering methods has been slow and the connection to a truly predictive theory has not yet been made.

## 2. Purpose of the present study

Most of the turbulent energy production takes place in the atmospheric surface layer (ASL), which occupies only a small fraction (about 10%) of the PBL. To get a better insight in the production and transport of turbulence in the ASL a field experiment was performed during daytime in which the occurrence of turbulent structures was investigated. The experiment contained turbulence measurements of wind velocity, air temperature and static pressure.

The measurement of turbulent static pressure fluctuations inside

the turbulent structures in the ASL, served another goal of this investigation, which was to resolve the mechanism of the origin and development of the turbulent structures.

The third aim of the present research was to obtain a comparison between the behavior of turbulent structures in the near neutral ASL and those in the laboratory turbulent shear layer.

### 3. Review of recent research

This review is rather concise and biased to the author's range of interest and views, and omits many detailed matters. However, it is hoped that it gives an impression of some of the main topics on which the current research is concentrated.

The Kansas experiments of 1968 (Haugen et al., 1971) provide a comprehensive picture of the structure of turbulence in the ASL. From these experiments it can be concluded that the mechanism of turbulent transport is not a continuous process but that the largest contributions to the turbulent transports are governed by coherent turbulent structures. Taylor (1958) already observed saw-tooth, or asymmetric ramp patterns in registrations of temperature at a height of 23 m. These ramplike patterns should be considered as a feature of large scale structures inside the turbulent flow. The exact nature of the large scale structure is not yet known satisfactorily.

Ensemble averages of turbulent velocities and temperatures obtained by the conditional sampling of turbulent structures in both the ASL and the laboratory turbulent shear layer closely resemble each other (Kaimal and Businger, 1970; Chen and Blackwelder, 1978; Phong-Anant et al., 1980). Also, greater turbulence intensities and a higher rate of momentum transfer is observed in both types of turbulent structures (Kim et al., 1971; Khalsa, 1980) and both are inclined to the surface.

Although the asymmetric temperature ramps in the ASL and the

laboratory turbulent shear structures show similarities, they are also fundamentally different in certain aspects. Perhaps the most significant difference is the merging of ramps into structures of more symmetrical shape above the ASL, which does not appear to have any counterpart in the laboratory (Wilczak and Tillman, 1980). The symmetrical structures extend through the entire PBL as the Minnesota data show (Kaimal et al., 1976). Thus in the PBL the size of the turbulent structures tends to increase while their number decreases with height, resulting in a smaller frequency of occurrence (Lenschow and Stephens, 1980).

There are still considerable gaps in the knowledge of various aspects of the structure of turbulence in the ASL, and many details remain to be elucidated by future investigations.

#### 4. Organization of the thesis

The kernel of this thesis consists of three chapters, which have been individually published or submitted as journal articles. To underline the individual identity of each chapter separate numbering of pages, equations and figures has been used.

In chapter II the definition of turbulent structures and a method to detect them in the ASL is presented. The turbulent structures are described in a qualitative manner. Chapter III contains a quantitative description of those turbulent structures which contribute most significantly to the vertical turbulent transports of momentum and heat. A mechanism of the formation of turbulent structures in the ASL has also been given. Chapter IV describes the dynamical properties of the turbulent structures in a near neutral ASL. Special attention has been paid to the role of turbulent static pressure fluctuations in the mechanism of the origin and development of the turbulent structures.

Throughout the chapters the present results have been compared with the results of experiments in laboratory turbulent shear layers.

## II. The detection and measurement of turbulent structures in the atmospheric surface layer \*

**Abstract** Turbulence data from the planetary boundary layer (PBL) indicate the presence of deterministic turbulent structures. These structures often show up as asymmetric ramp patterns in the measurements of the turbulent fluctuations of a scalar quantity in the atmospheric surface layer (ASL). The sign of the slope of the sharp upstream edge of such a triangular pattern depends on the thermal stability conditions of the ASL.

The turbulent structures in the ASL have been tracked by a detection method which searches for rapid and strong fluctuations in a signal - the VITA (variable interval time averaging) technique. This detection method has previously been employed in laboratory boundary layers. The VITA detection method performs well in the ASL and reveals the presence of vertically coherent turbulent structures, which look similar to those in laboratory shear flows. At the moment that a sharp temperature interface appears, the horizontal alongwind velocity shows a sharp increase, along with a sudden decrease of the vertical velocity, independent of the thermal stability conditions of the ASL. The fluctuating static pressure reveals a maximum at that moment. The vertical turbulent transports show a twin-peak character around the time that the sharp jumps in the temperature and the velocity signals appear.

\* Published in Boundary-Layer Meteorology 29 (1984) 39-58.

## 1. Introduction

Turbulence has long been described by its statistical properties only, for example its mean, variance, probability distribution and power spectral density function. A few decades ago, laboratory experiments were performed in order to visualize turbulent flows. The results of these investigations indicated that a turbulent flow contained organized, spatially coherent motions, i.e. structures. These turbulent structures are central to understanding the mechanism of turbulence. They play an important role in the processes of production and transport of turbulence. The transport of mass, momentum and heat in a turbulent boundary layer does not occur continuously. Time intervals appear during which very intensive transport, contained in the structures, takes place, and other time intervals appear during which very little transfer occurs.

Laboratory visualization experiments demonstrated that turbulent structures, on the average, were regularly distributed in the flow field. However, the instantaneous distribution of the structures varied from one instant to another. The laboratory experiments were carried out under well controlled conditions in wind- or water-channels along either aerodynamically smooth or rough boundaries.

The question arises whether the cyclic structures observed in the laboratory also appear in the ASL. Turbulent kinetic energy is produced through the action of the shear stresses present in boundary-layer flows. Therefore, laboratory and atmospheric shear flows, the latter under neutral conditions, can be expected to show common characteristics. It is reasonable to suppose that the structures observed in laboratory shear flows also occur in a neutral ASL. In a non-neutral ASL, the buoyancy can act as a source or sink of turbulent kinetic energy. In a daytime PBL, the thermally unstable stratification causes convective motions to develop. Thus, it may be expected that during the daytime when

the atmosphere is unstable, both shear and buoyancy forces will cause turbulent structures.

In order to find out how turbulent structures behave, they have to be tracked and conditionally sampled. This means that one observes the values of the flow quantities inside the structures. In order to perform such conditional sampling properly, a detection scheme has to be used which unambiguously reveals the presence of turbulent structures. The major trouble with turbulence signals, in general, is that the flow patterns which are to be recovered are buried in background turbulence, which has roughly the same frequency of occurrence and amplitude distribution as these flow patterns.

In section 2 a description is given of turbulent structures in the ASL, which have been tracked by visual inspection. The results of using the VITA technique to measure turbulent structures in the ASL are discussed in Section 3. In section 4 some conclusions are finally drawn and recommendations are made for future research. Turbulent structures will be defined as spatially coherent, organized flow motions. 'Organized' means that characteristic patterns, observed at a point in space, occur almost simultaneously in more than one turbulence signal and are repeated periodically.

## 2. The present investigation

Turbulence data were gathered at two different sites. One set of data was provided by the Royal Netherlands Meteorological Institute (KNMI). These data were obtained at a meteorological tower of the KNMI, near the village of Cabauw, located in the central river delta of the Netherlands (see Driedonks et al., 1978 for an extensive description). The data consist of turbulence measurements of wind velocities, air temperatures and humidity mixing ratios between heights of 20 and 200 m on August 26 and 27, 1976 and on May 30, 1978 (see Driedonks et al., 1980 for

Table I Description of the data

Run designation of the analyzed data. Values of sampling rate ( $f_s$ ), the number of samples (N), the Obukhov length (L), lowest inversion height ( $z_i$ ), measuring height (z), mean wind velocity ( $\bar{u}_z$ ), azimuth angle ( $\bar{\theta}_z$ ) and mean temperature ( $\bar{T}_z$ ) are listed.

Run	location	date	time (GMT)	$f_s$ (s <sup>-1</sup> )	N	L (m)	$z_i$ (m)	z (m)	$\bar{u}_z$ (ms <sup>-1</sup> )	$\bar{\theta}_z$ (deg)	$\bar{T}_z$ (°C)
KA 26	KNMI-site	8/26/76	1700- 1800	2	7150	∞*	1181 <sup>‡</sup>	20	5.28	7.2	18.1
KA 27	KNMI-site	8/27/76	1300- 1400	2	7150	-600	2238 <sup>‡</sup>	20	9.65	16.3	20.6
KA 30	KNMI-site	5/30/78	1420- 1510	5	14995	- 59	750 <sup>+</sup>	20	3.89	71.3	25.3
LA 28	IH-site	4/28/83	1509- 1520	12.5	8275	-422	880 <sup>‡</sup>	40	4.27	75.4	25.5
								80	4.57	76.6	25.0
								120	4.78	72.8	24.2
								160	5.05	80.5	24.0
								200	5.35	85.9	23.5
								3.56	5.8	217	11.7
								9.56	6.7	217 <sup>□</sup>	11.4

Notes:

\* ∞ means  $|L| > 5000$  m, where  $L = \frac{-u_*^3}{\text{kg } w^* T' / \bar{T}}$

<sup>‡</sup> estimated from  $z_i \approx 0.25 u_* / 1.1 \cdot 10^{-4}$  (see Tennekes, 1970)

+ measured at 1115 GMT (see Driedonks, 1981)

□ estimated from value at other height.

a complete description of this data set).

The other set of data was collected during the spring of 1983 by the author and members of the Department of Physics and Meteorology of the Agricultural University of Wageningen (LHW). The experiments were performed at the meteorological site of the Minderhoudhoeve near Swifterband in the Oostelijk-Flevoland polder, which is located in the central part of The Netherlands. These turbulence data contain wind velocities, air temperatures and static pressure fluctuations, measured in the lowest 10 m of the surface layer on April 28, 1983. (A complete description of this measuring program is in preparation).

Table I contains a general description of the data.

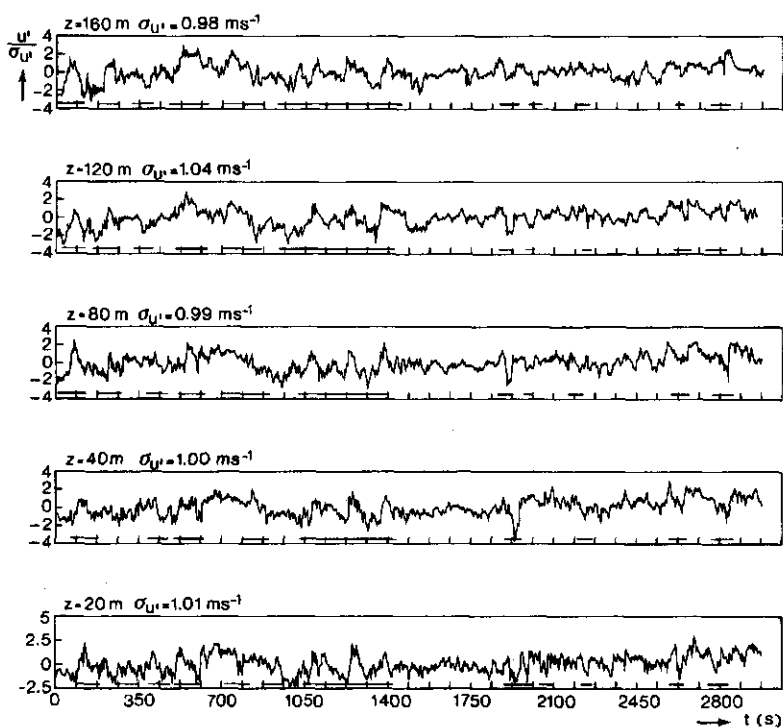
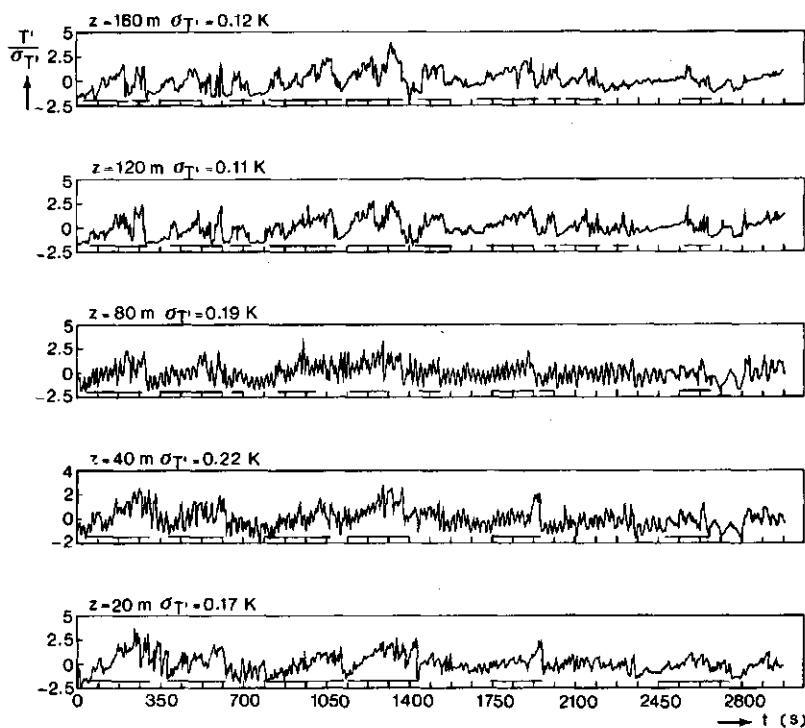
Figure 1.a presents a graph of turbulent temperature fluctuations ( $T'$ ) which were measured simultaneously at five different heights during the afternoon of May 30, 1978 (KNMI site). Periods occur during which the fluctuations are vertically coherent as indicated by the horizontal bars. These large-scale patterns appear as above the mean fluctuations. Approaching the surface they become more like skewed ramplike patterns due to the increasing influence of the wind shear. The patterns at lower levels lag the higher ones, indicating that the patterns are tilted in the direction of the mean wind.

The alongwind velocity fluctuations ( $u'$ ) presented in Figure 1.b also show vertically coherent flow patterns. They are, however, less prominent than in the temperature records. The periods during which both velocity and temperature traces show vertical coherence roughly agree with each other. During these periods the flow contains turbulent structures, which modulate both velocity and temperature fluctuations.

Turbulent fluctuations of the mixing ratio ( $r'$ ) and temperature ( $T'$ ), both being scalar quantities, behave identically as indicators of the large-scale structures. This is shown in Figure 1 c.

Figure 2 shows another set of turbulence data, measured around noon on August 27 at 20 m height (KNMI site). The ramp patterns (indicated by the horizontal bars) in the temperature trace appear on a variety of scales. They are often accompanied, at their upstream ends, by high values of the vertical turbulent transports, which fluctuate intermittently throughout the entire length of the observation. A necessary condition, in order to infer that large transports occur, is that the turbulent velocities and temperatures show large departures from their zero means simultaneously. Figure 2 shows that this also happens during intervals when no distinct asymmetric ramp pattern is visible in the temperature record, but when the temperature trace shows a 'top hat' shape (indicated by chained bars). Within these intervals, the transport is not concentrated at the upstream end, but is more evenly distributed along the time intervals. At one interval (indicated by a dotted line denoted with an 'a') a ramp pattern is captured inside a 'top hat' pattern. The turbulent transport often shows a double peaked character (denoted by symbols 'e' and 's') at the upstream interface of a temperature ramp. Such behavior of the  $u'w'$ -crossproduct has also been observed in the laboratory (Blackwelder and Kaplan, 1976, p. 107; Subramanian et al., 1982, p. 354) and is called a 'burst event'. It has been explained as a sweep ('s') following an ejection ('e') inside a turbulent structure. A laboratory turbulent structure consists of four phases. First, fluid near the wall boundary is retarded and lifted, and a layer of low speed fluid (streak) builds up. Second, oncoming fluid from upstream, having a higher speed, causes a shear layer between itself and the low speed wall fluid. Third, increasing shear causes a sudden break-up of the wall streak during which violent ejection of the wall fluid takes place (bursting). Finally, the wall streak is quickly replaced by high-speed fluid (sweep) from the outer region of the boundary layer. The whole cycle then repeats.

From the foregoing results, it may be deduced that the PBL contains turbulent structures which penetrate into the ASL where they modulate both velocity and temperature traces and show



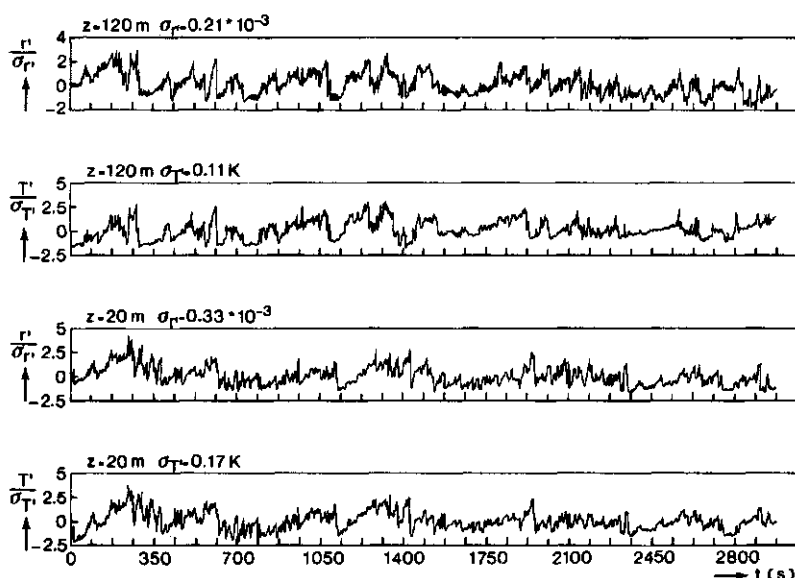


Figure 1 Simultaneous measurements of turbulent temperature fluctuations ( $T'$ ), fluctuations of horizontal velocity in the forward direction ( $u'$ ) and variations of mixing ratio ( $r'$ ) at different heights. Data are normalized by their standard deviation ( $\sigma$ ), and are from Run KM 30.

characteristics which are common to turbulent structures in the laboratory shear layer. The asymmetric ramp patterns in the temperature signals tracked by visual inspection in the ASL correspond to those observed by several other investigations (Taylor, 1958; Kaimal and Businger, 1970; Antonia et al., 1979; Phong-Anant et al., 1980). They have also been observed in laboratory shear flows (Chen and Blackwelder, 1978).

### 3. Results of the use of the VITA detection technique to measure turbulent structures in the atmospheric surface layer

To track the turbulent structures in the ASL in an objective way, one has to look for one or more features characteristic of a turbulent structure which uniquely reveals its presence in the back-

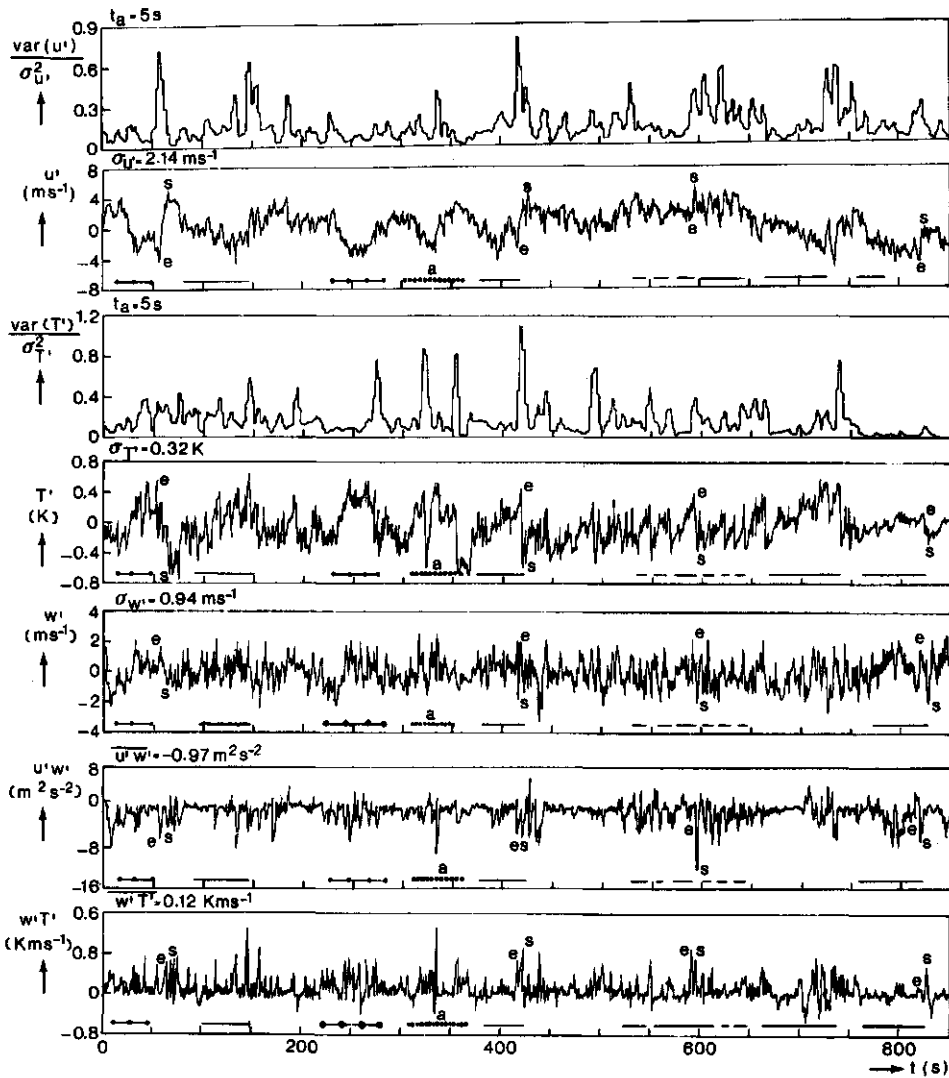


Figure 2 Turbulent fluctuations of horizontal velocity in the forward direction ( $u'$ ), vertical velocity ( $w'$ ), temperature ( $T'$ ) and instantaneous turbulent kinematic vertical transports of horizontal windwise momentum ( $u'w'$ ) and heat ( $w'T'$ ). Long-time averages are denoted by a horizontal bar above a quantity. The normalized short-time variance signals of temperature and horizontal velocity in the forward direction are also presented (Run KA 27).

ground turbulence. In Section 2 it was shown that most of the turbulent intensity is contained inside turbulent structures, which often manifest as asymmetric triangular shapes with a sharp upstream interface in the temperature records in the ASL. It seems straightforward, therefore, to check for rapid and strong fluctuations in a single turbulence signal. When this is done, using the VITA detection technique with the present data, the results reveal the features that are generally accepted for the description of the turbulent structures.

The VITA technique is based on a very simple flow concept and thus is easily applied. Subramanian et al. (1982) have shown that of various one-point detection schemes, the VITA method correlated best with a visual detection technique for coherent structures, based on examination of simultaneous temperature traces from a rake of cold wires inside a laboratory boundary layer. The VITA detection technique was first introduced by Kaplan and Laufer (1968) in order to study the structure associated with the motion of the turbulent/non-turbulent interface in the outer part of a laboratory boundary layer. The VITA method has been used here with minor modifications (cf. Chen and Blackwelder, 1978). The detection scheme computes a short-time variance signal, normalized by the long-time variance. When the normalized short time variance exceeds some specified threshold level ( $k$ ), and the slope of the short-time averaged fluctuations satisfies an additional criterion, an 'event' is said to occur. The normalized short-time variance signal, as also presented in Figure 2, is defined as

$$\frac{\text{var}(d')}{\sigma_{d'}^2} = \frac{1}{2} \left\{ \frac{1}{t_a} \int_{t-\frac{1}{2}t_a}^{t+\frac{1}{2}t_a} d'^2 ds - \left( \frac{1}{t_a} \int_{t-\frac{1}{2}t_a}^{t+\frac{1}{2}t_a} d' ds \right)^2 \right\}$$

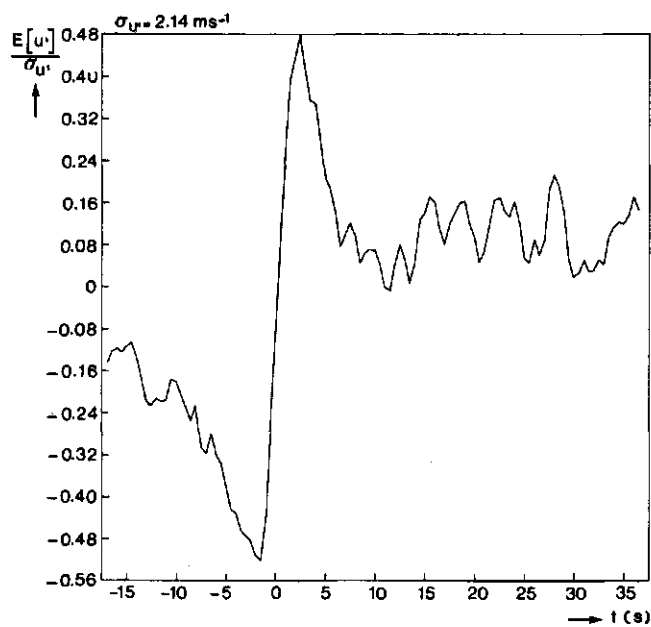
The averaging procedure acts roughly as a low-pass filter, accepting frequencies below  $1/t_a$ , where  $t_a$  denotes the length of the short averaging time.  $d'$  stands for the fluctuating turbulent detection signal and  $\sigma_{d'}^2$  denotes its long time variance.

A significant property of the VITA method is that it acts as a bandpass filter which passes time scales of the order of  $t_a$ . Johansson and Alfredsson (1982) found that the VITA method picks out those 'events' with a time scale of about  $1.3 t_a$ , where the time scale of an 'event' is taken as twice the width of the sharp fluctuation which has been detected.

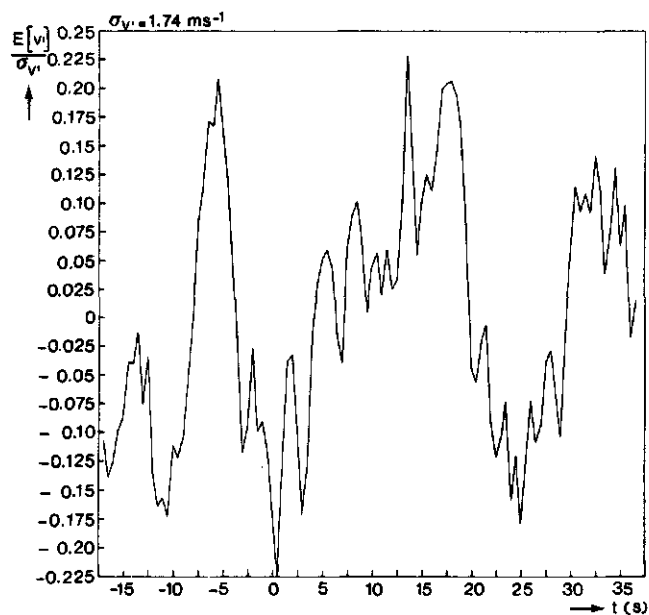
In an unstably stratified ASL (such as the KNMI data presented thus far), the temperature is used as a detection signal, since its signal-to-noise ratio is larger than that of the velocity signal, viz. the ramp patterns possess a markedly higher temperature than outside. The slope criterion is chosen negative with respect to time, since the ramps are marked by an abrupt decrease in temperature at their upstream end.

Figure 3 presents some conditional averages ( $E[f']$ ), which are basically ensemble-averaged turbulence signals ( $f'$ ) around the time that a detection occurs. In Figure 4 ensemble-averages are shown of turbulence data which were measured in a slightly stable ASL (during the evening of August 26 on the KNMI site). This is indicated by the inverted ramp patterns in the conditionally averaged temperature signal (cf. Figure 4c). The detection signal was defined as the horizontal alongwind velocity fluctuation, and not the temperature, because the signal-to-noise ratio for the velocity signal was higher than for the temperature signal. The slope criterion was chosen positive with respect to time, since the 'events' appeared to be marked by a sharp acceleration of the  $u'$  velocity. Van Maanen and Fortuin (1983) used a similar detection criterion in a turbulent pipe flow.

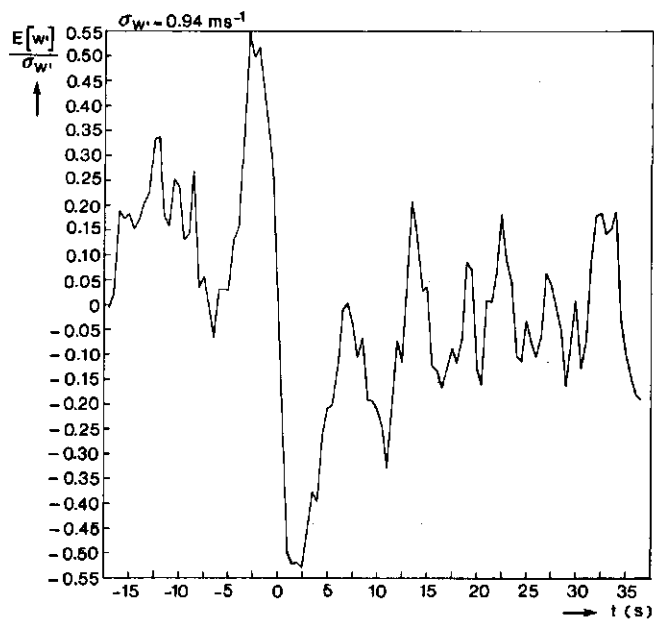
From the definition of the short-time variance and the threshold level, it can be inferred that the mean amplitude of the detected 'events' is proportional to the square root of the threshold level. The ensemble averages in Figure 4, which are normalized by  $\sigma_f/\sqrt{k}$  confirm this suggestion. The virtual collapse of the ensemble-averaged data into a single curve indicates that the variation of the threshold level only affects the magnitude and not the character of the detected 'events'. Such a picture was also



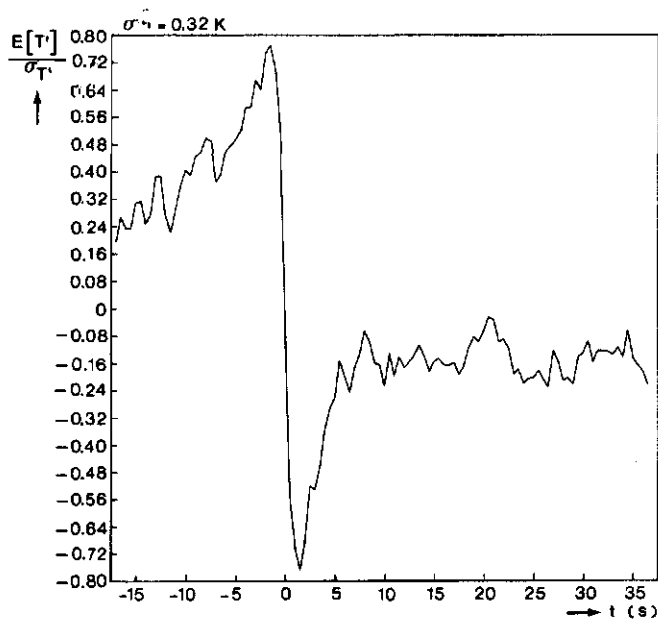
a



b

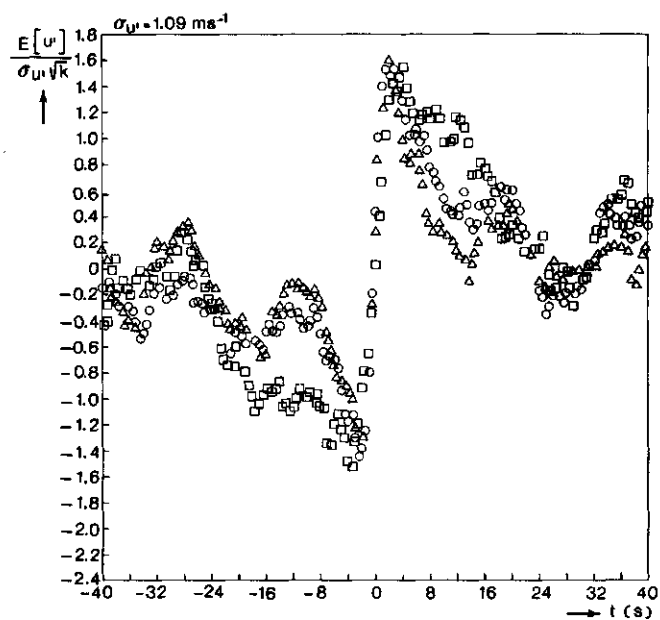


c

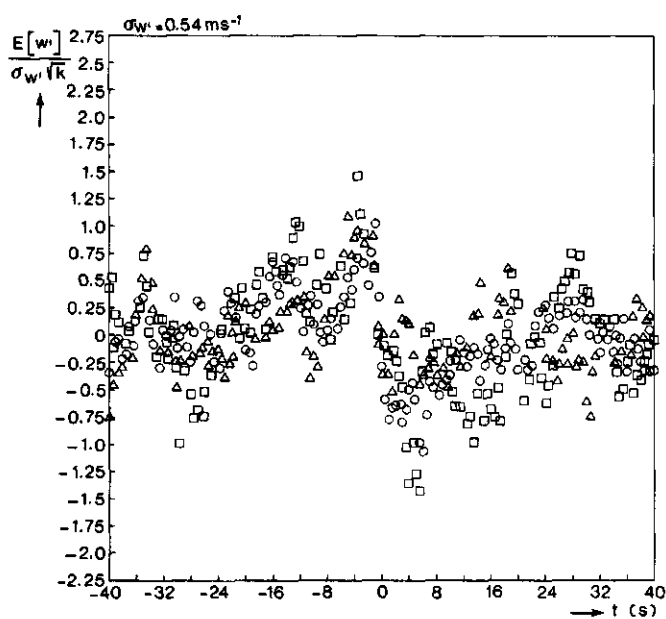


d

Figure 3 Conditional averages of  $u'$ ,  $v'$ ,  $w'$  and  $T'$  turbulent signals from Run KA 27. The temperature has been used as detection signal, while the slope criterion is negative  $t_a = 5s$ ,  $k = 0.4$ ,  $n = 56$ .



a



b

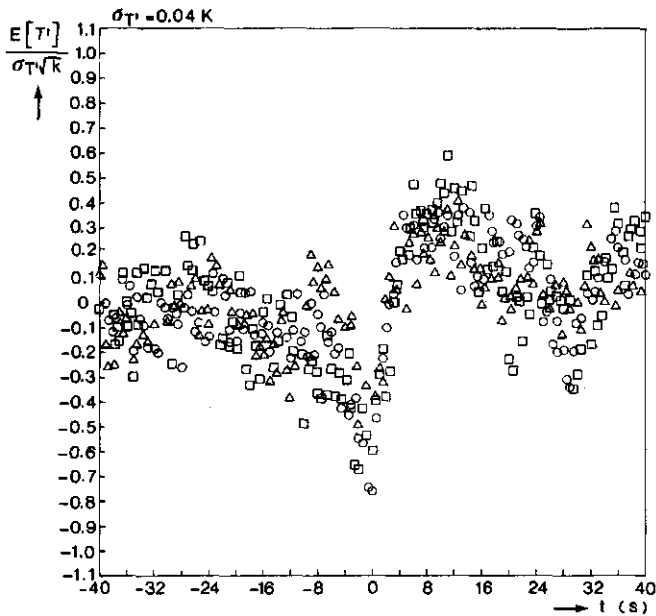


Figure 4 Conditional averages of  $u'$ ,  $w'$  and  $T'$  turbulent signals, normalized by the square root of the threshold level ( $k$ ). The short averaging time  $t_a$  is taken as 5 s. The horizontal alongwind velocity signal is taken as detection signal, while the slope criterion is taken to be positive. (Run KA 26).

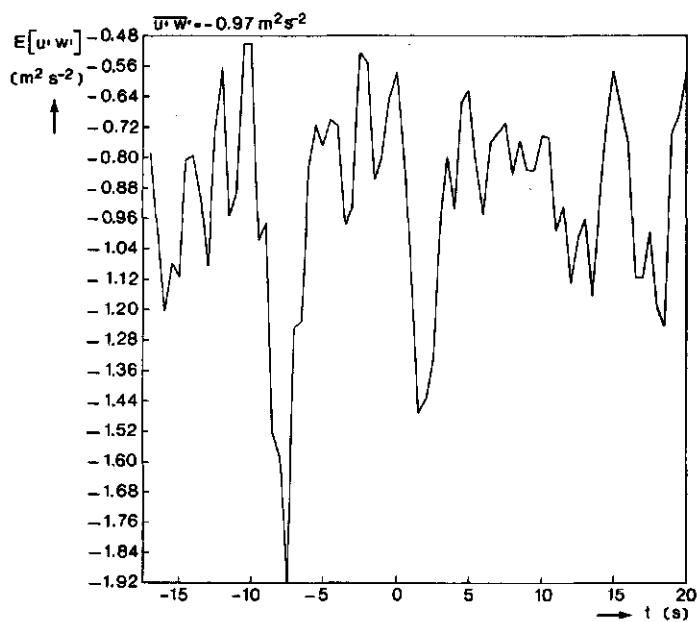
□  $k = 0.1$ ,  $n = 61$

△  $k = 0.3$ ,  $n = 47$

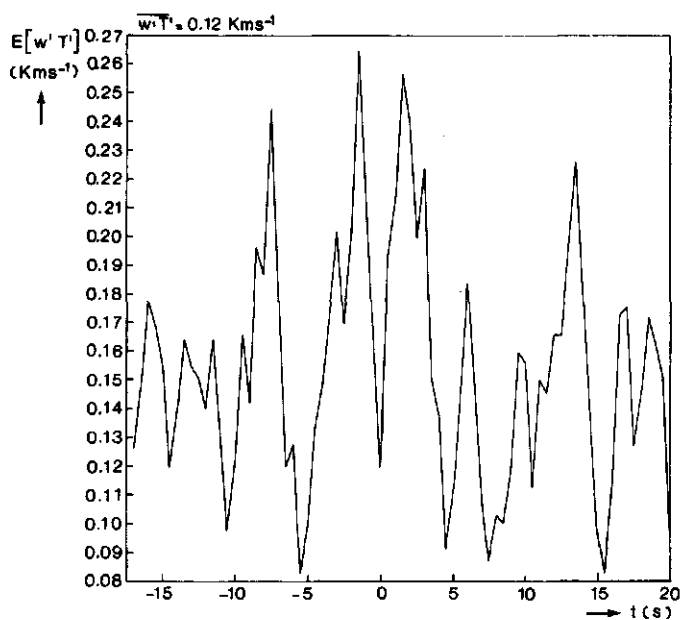
○  $k = 0.5$ ,  $n = 22$ .

found in the laboratory (Blackwelder and Kaplan, 1976, p. 111; Johansson and Alfredsson, 1982, pp. 307 and 309).

During an average 'event', the horizontal velocity in the forward direction ( $u'$ ) shows a rapid increase, after a slow decrease. The vertical velocity ( $w'$ ) shows a fast decrease, after an increase. The general shapes of both patterns, as shown in Figures 3 and 4, are independent of the thermal stability condi-



a



b

Figure 5 Conditional averages of the turbulent kinematic vertical transports  $u'w'$  and  $w'T'$  for the data from Run KA27.  $t_a = 5s$ ,  $k = 0.4$ ,  $n = 56$ .

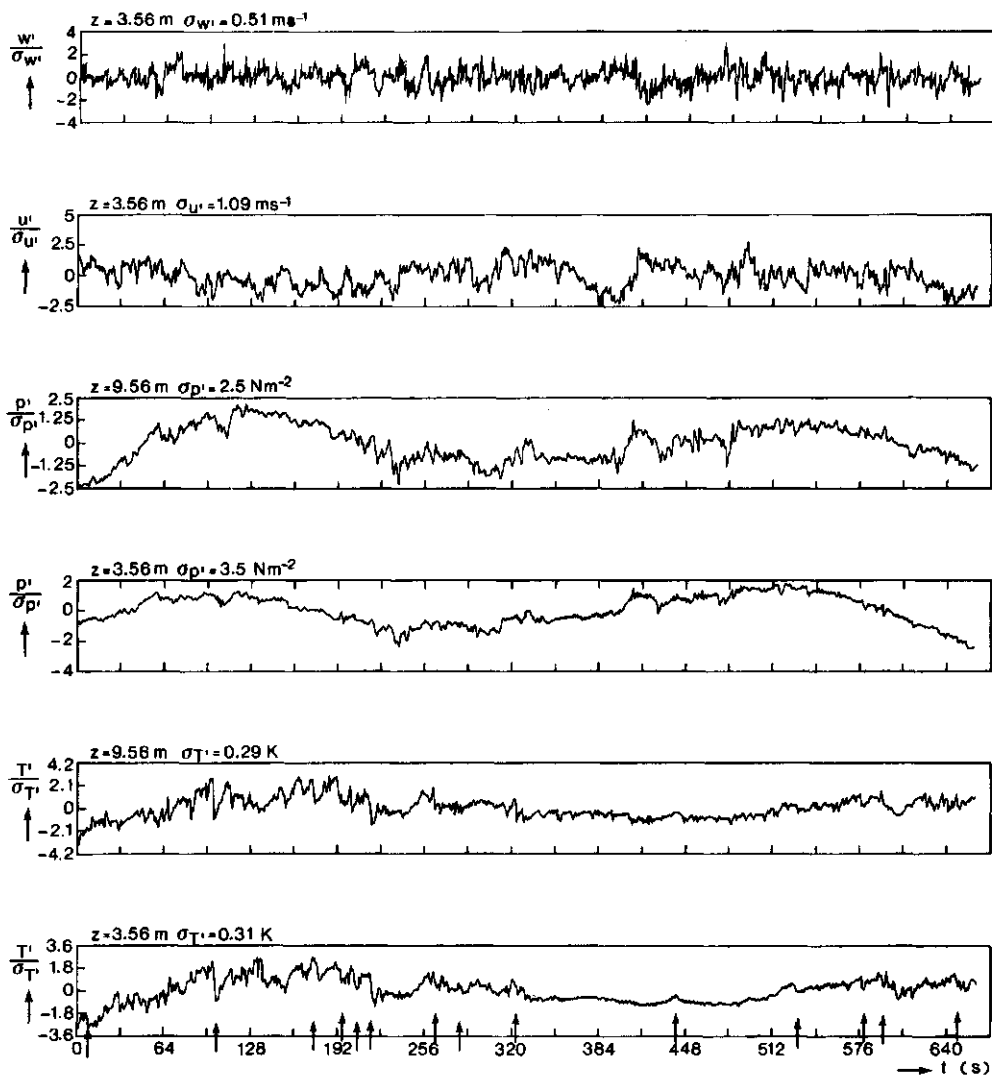


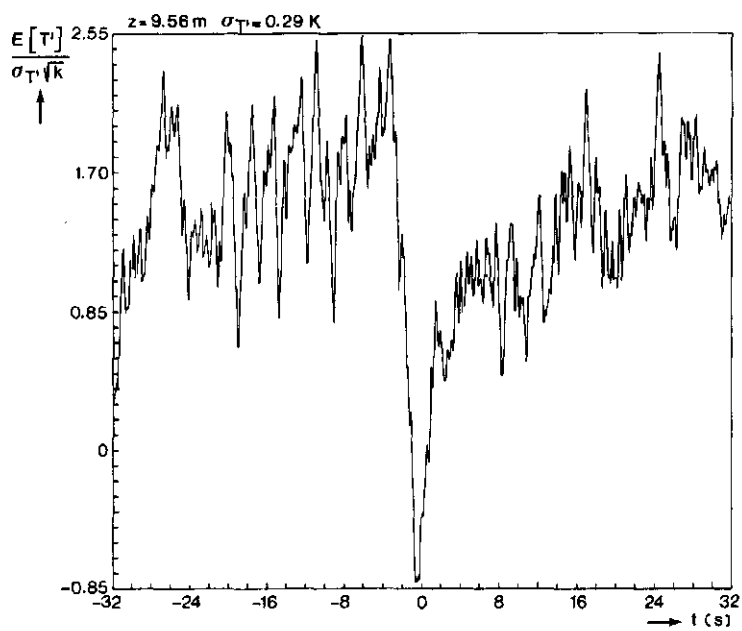
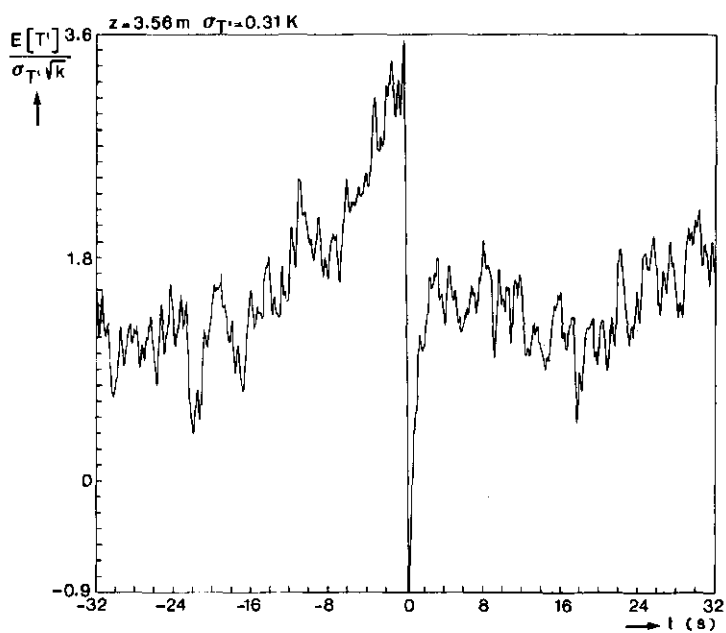
Figure 6 Simultaneous records of turbulent fluctuating signals measured on the LHW site (Run LA 28) at heights ( $z$ ) of 3.56 and 9.56 m. The data have been smoothed by a moving average over 11 points.

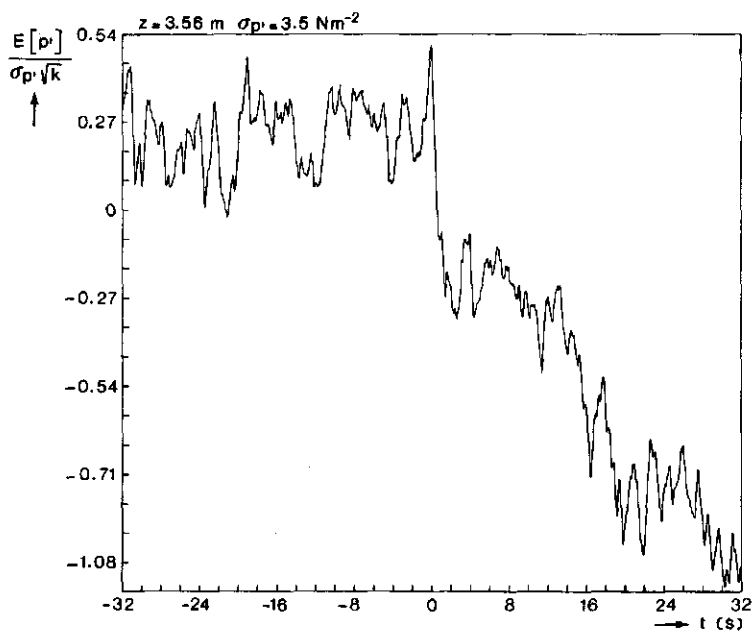
tions in the ASL. The conditionally averaged horizontal cross-wind velocity fluctuations ( $v'$ ) show no particular pattern during an 'event' (cf. Figure 3b).

Around the so-called reference time ( $t = 0$ ), i.e. the time that the sharp jumps in the various turbulent signals occur, the ensemble-averaged  $u'w'$  cross product ( $E[u'w']$ ) displays a twin-peak character, as illustrated in Figure 5a. The conditionally averaged turbulent vertical kinematic heat flux ( $E[w'T']$ ) shows a double peaked character around  $t = 0$  as well (cf. Figure 5b). However, for the slightly stable ASL data, this behavior is less apparent. This may be due to the near neutral character of the ASL, in which the average turbulent heat flux has a very small negative magnitude and is mainly determined by small-scale fluctuations.

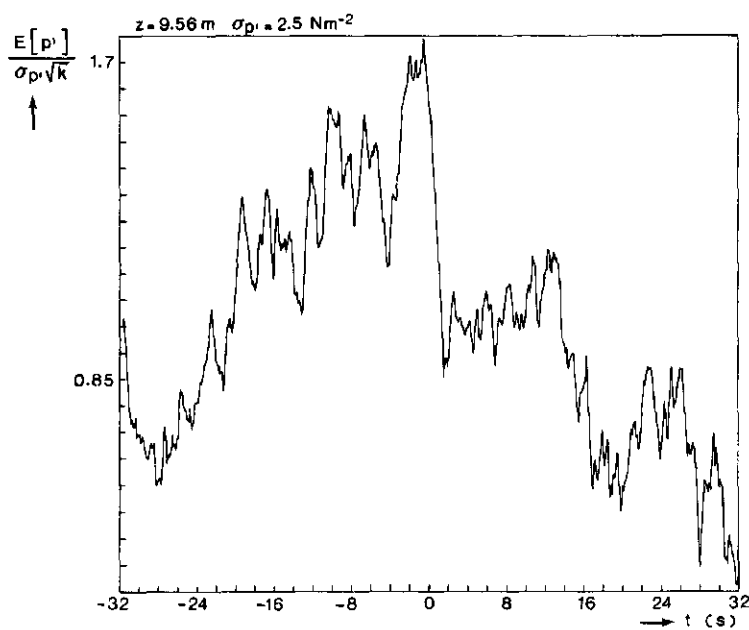
In Figure 6 a series of turbulent signals, measured late in the afternoon of April 28, 1983 (LHW site) is presented. The graphs show turbulent velocities, temperatures and static pressure fluctuations ( $p'$ ) measured at 3.56 and 9.56 m heights. The static pressure fluctuations were measured with a probe designed by Elliott (1972a) and built by members of the Department of Physics and Meteorology of the LHW. (A complete description of the pressure probe is in preparation). The VITA technique has been applied to these unstable ASL data. The resulting conditional averages are shown in Figure 7. These ensemble averages reflect the properties that are accepted for the recognition of turbulent structures: the coherent temperature ramp patterns at the two levels, and the presence of characteristic patterns in the along-wind horizontal velocity fluctuations and the vertical turbulent velocity. The phase shift between the temperature interfaces at the two height levels (cf. Figure 7a and b) indicates that the ensemble - averaged turbulent structure is inclined to the surface.

The patterns in the static pressure fluctuations around  $t = 0$  (cf. Figures 7c and d) resemble those described by Thomas and Bull (1983), who measured wall pressure variations in a labora-

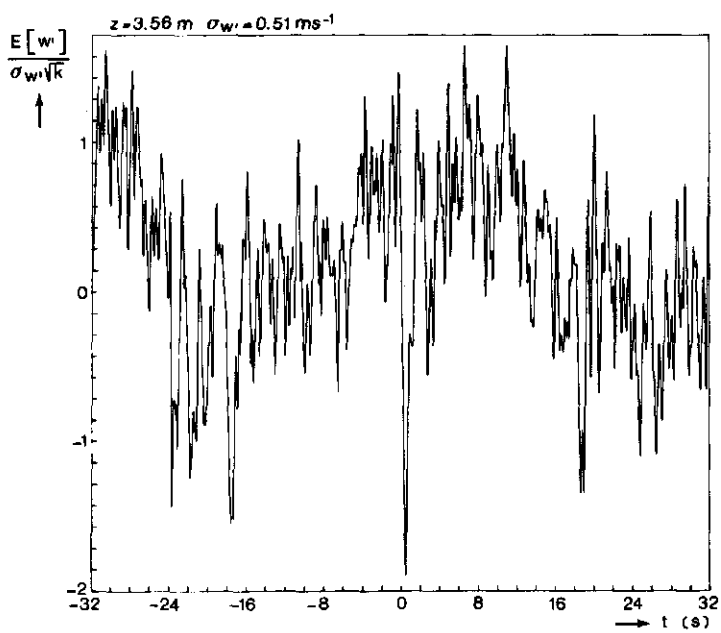
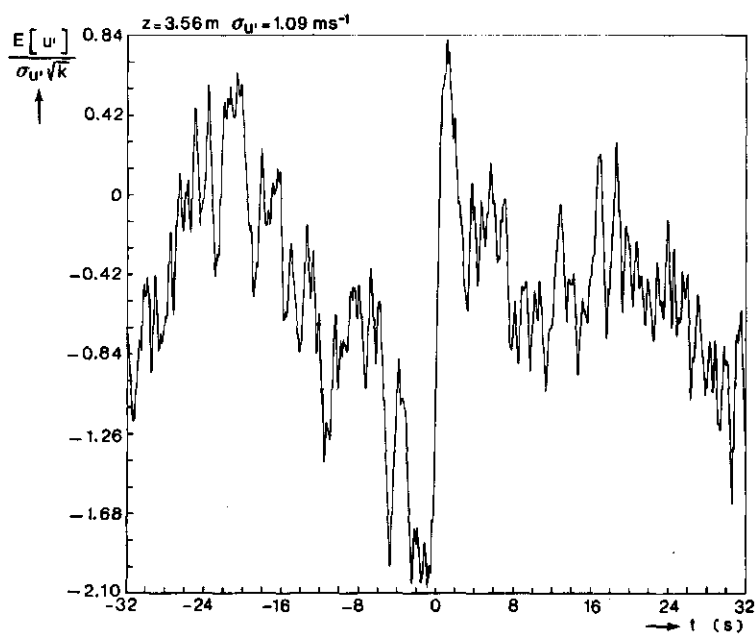




[c]



[d]



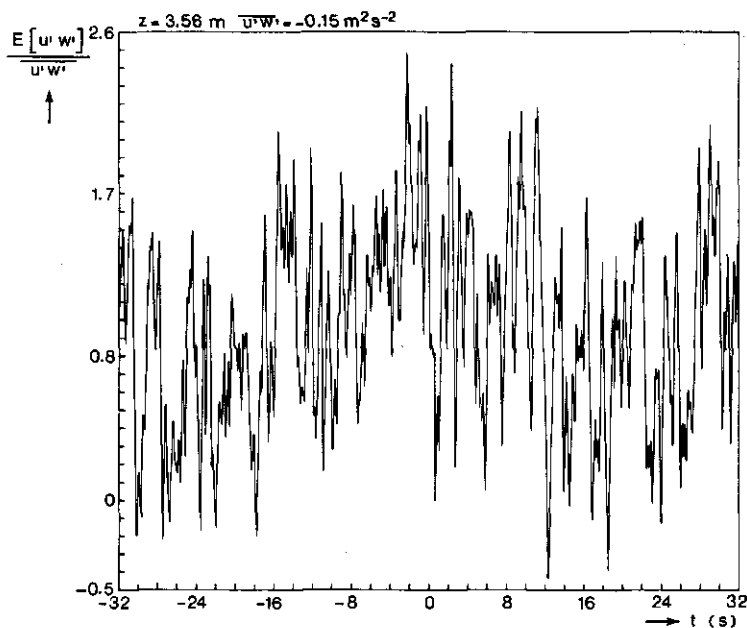


Figure 7 Conditionally averaged  $T'$ ,  $p'$ ,  $u'$  and  $w'$  turbulence data from Run LA 28. The temperature at 3.56 m height has been taken as detection signal while the slope criterion has been chosen to be negative.  $t_a = 0.8$  s,  $k = 0.1$ ,  $n = 23$ .

tory boundary layer. The vertically coherent pressure patterns are maximum at the sharp interface of the turbulent structure, which may be identified with the 'burst event' in a laboratory shear layer.

The conditionally averaged quantity  $u'w'$  (cf. Figure 7g) is higher than average around  $t = 0$ . Near  $t = 0$  it is close to zero, but it does not show a twin-peak behavior as pronounced as in the KNMI data. On the one hand, this may be due to the phase-shift error caused by the spatial separation of the sonic anemometer sensors, used to measure the velocity components. On the other hand, these data show many high-frequency fluctuations, which disturb the large-scale patterns characteristic of turbu-

II.22

lent structures. The turbulent vertical kinematic heat flux is also poorly determined because of its small magnitude.

The records in Figure 6 show the presence of individual turbulent structures, in which the features described above show up; they are indicated by vertical arrows on the lower axis.

The performance of the VITA detection technique is satisfactory, when applied to ASL turbulence data. The qualitative behavior of the conditional averages, using this method, is not sensitive to the selection of the detection parameters, i.e. threshold level and short averaging time.

#### 4. Conclusions

Results of conditional averaging of turbulence data from the atmospheric surface layer (ASL) clearly indicate a deterministic flow behavior in which turbulent structures are present. In the time traces of a scalar quantity, such as the temperature or mixing ratio, these structures are manifest often as asymmetric triangular shapes with a sharp upstream edge. The sign of the slope of that interface depends on the thermal stability conditions of the atmospheric boundary layer.

The turbulent structures are objectively detected by means of the VITA detection technique, which looks for rapid and strong fluctuations in a single turbulent signal at one point in space. The detected 'events' show, at the moment that the sharp temperature interface occurs, a sudden increase of the horizontal velocity in the forward direction, along with a sudden decrease of the vertical velocity, independent of the thermal stability conditions of the ASL. This is indicative of the presence of a so-called internal shear layer, as has already been observed at the upstream edge of turbulent structures in laboratory shear flows (cf. Chen and Blackwelder, 1978). Furthermore, this dynamic flow behavior has already been observed in the ASL by Phong - Anant et al.(1980)

who selected the turbulent structures by visual inspection.

At the moment - the reference time - that the sharp temperature interface appears, the fluctuating static pressure shows a maximum. This organization is also tracked in the conditionally averaged turbulent shear stress, which shows a twin-peak character around the reference time. Such a double-peaked character has already been observed in laboratory flows and has been explained as a sweep following an ejection inside a turbulent structure. The ensemble-averaged  $w'T$  signal shows a similar behavior, also being relatively small at reference time and relatively large just before and just after it. The turbulent structures contain much of the turbulent intensity. The Kansas experiments of 1968 (Haugen et al., 1971) showed that the largest contributions to the turbulent transports in the ASL were governed by vertically coherent turbulent structures.

The present turbulence data set are being used to study the relationship of turbulent structures to their environment, such as translation velocity, inclination angle to the surface, spatial distribution and temporal behavior. The results, together with quantitative data on the contribution of turbulent structures to the turbulent transport processes, will be presented in a forthcoming paper.

An interesting aspect to be studied is to find, if possible, some links between the scaling of turbulent structures in the laboratory and in the ASL. The exact role of static pressure fluctuations inside the turbulent structures in the ASL has to be resolved in order to understand the mechanism of the origin and development of structures.

### III. Characteristics of turbulent structures in the unstable atmospheric surface layer \*

**Abstract** An atmospheric surface layer (ASL) experiment conducted at a meteorological site in the Oostelijk-Flevoland polder of the Netherlands is described. Turbulent fluctuations of wind velocity, air temperature and static pressure were measured, using three 10 m towers.

Traces of simultaneous turbulent signals at several heights on the towers were used to investigate the properties of the turbulent structures which contribute most significantly to the turbulent vertical transports in the unstable ASL. These turbulent structures produce between 30 and 50 percent of the mean turbulent vertical transport of horizontal alongwind momentum and they contribute to between 40 and 50 percent of the mean turbulent vertical heat transport, both during 15 to 20 percent of the total observation time.

The translation speed of the turbulent structures equals the wind speed averaged over the depth of the ASL, which scales on the surface friction velocity. The inclination angle of the temperature interface at the upstream edge of the turbulent structures to the surface is significantly smaller than that of the internal shear layer, which is associated with the temperature interface. The turbulent structures in the unstable ASL are determined by a large scale temperature field: Convective motions, which encompass the whole depth of the planetary boundary layer (PBL), penetrate into the ASL. The curvature of the vertical profile of mean horizontal alongwind velocity forces the alignment of the convective cells in the flow direction (Kuettner, 1971), which have an average length of several hundreds of metres and an average width of a few tens of metres. This mechanism leads to the formation of turbulent structures, which extend throughout the depth of the ASL.

\* Accepted by Boundary-Layer Meteorology with A. Jansen and

J. Krom as co-authors.

III.1

## 1. Introduction

A large part of the turbulent vertical transports of heat and momentum in the ASL is contained in turbulent structures, which are defined as spatially coherent, organized flow motions (Schols, 1984). The contribution of the turbulent structures to the turbulent transport processes has been quantified for unstable ASL data. These turbulence data were gathered at a meteorological site of the Agricultural University of Wageningen (LHW). Section 2 contains a description of the site and data-acquisition procedure.

The relationship of the turbulent structures to their environment has been investigated and has been presented in terms of their temporal behavior and spatial distribution. The results, together with the quantitative data on the contribution of the turbulent structures to the turbulent transport processes, are presented in Section 3.

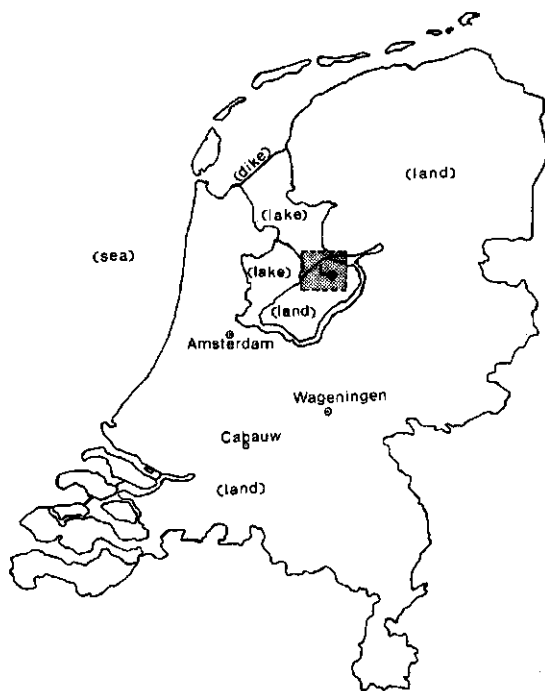
In Section 4 a formation mechanism for the turbulent structures in the unstable ASL is presented.

## 2. Experimental details

The turbulence data were collected during the spring of 1983, and contain wind velocities, air temperatures and static pressure fluctuations, measured in the lowest 10 m of the ASL. The experiments were performed at the meteorological site of the Minderhoudhoeve near Swifterbant in the Oostelijk-Flevolandpolder, which is located in the central part of the Netherlands (Figure 1).

### 2.1 Site and instrumentation

The LHW-site is situated at about  $52^{\circ} 33'N$  and  $5^{\circ} 40'E$  (cf. Figure 1). The area is almost flat: local relief variations are



0 20 40 60 80 100 km

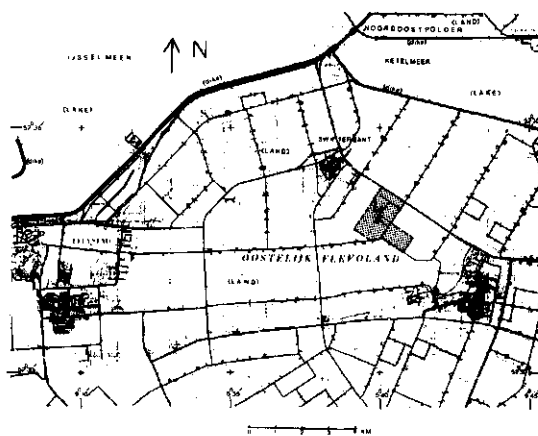


Figure 1 Location (L) of the experimental site

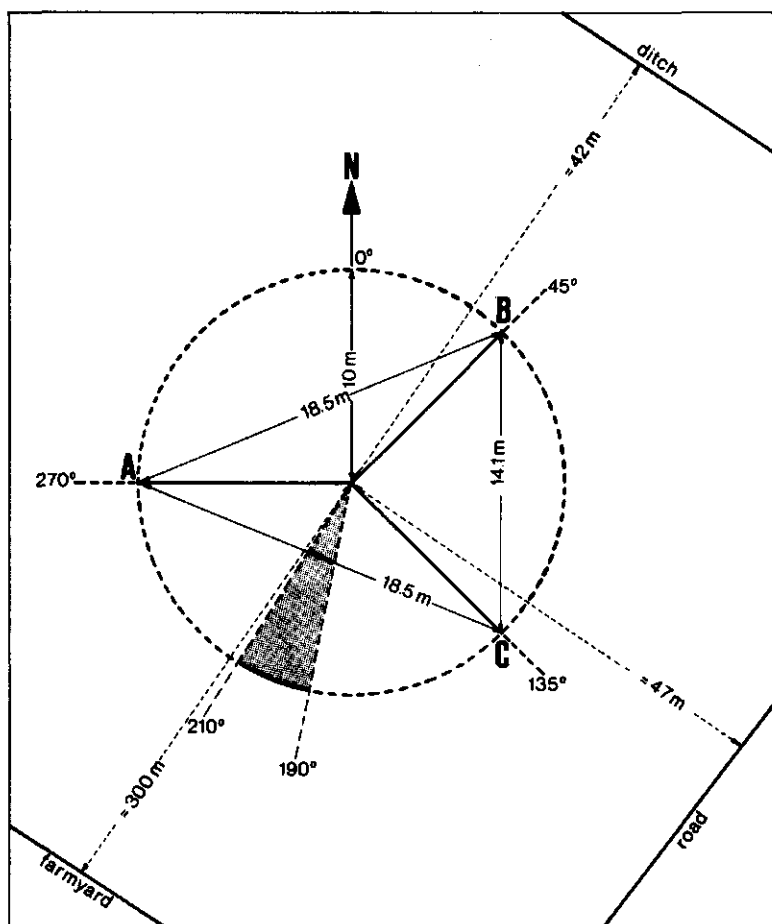


Figure 2 Ground plan of the array of 10 m towers, indicated by the characters A, B and C.

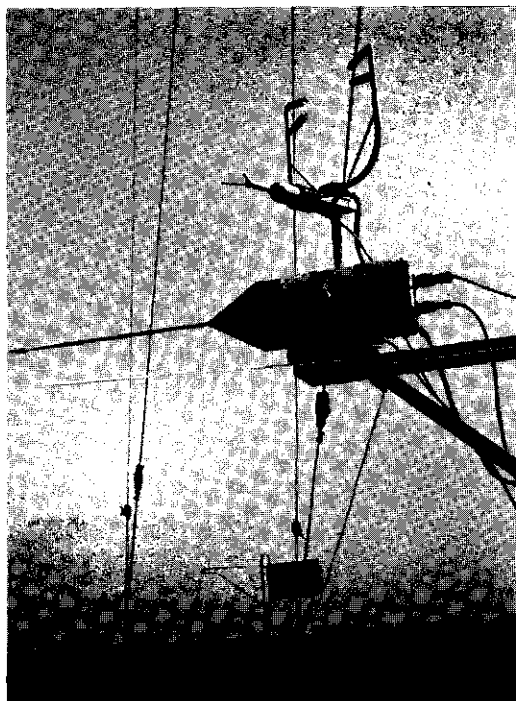
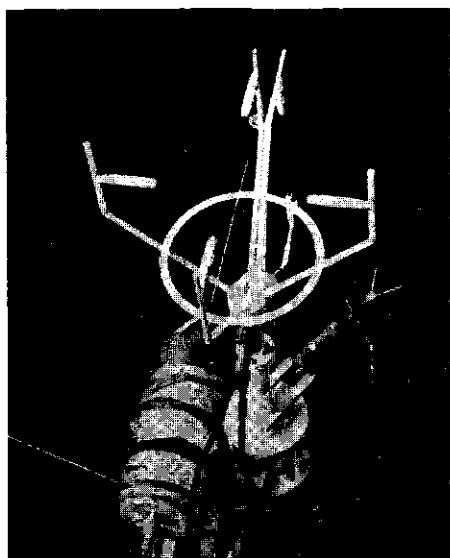


Figure 3 Close-up of sensors on a tower.  
The static pressure sensors and the inclinometers  
were each mounted on a small platform. The sonic  
anemometers and the V-shaped thermometers were at-  
tached to a post on top of the inclinometers.

less than about 10 cm per kilometre in all directions, apart from dikes and canals which respectively are about a few metres high and a few metres deep. During the experiments, the ground cover basically consisted of grassland about 10 to 20 cm high. The roughness length of the ground surface was about 2 cm, which was obtained by assuming a logarithmic wind profile for high velocities at near neutral thermal stability conditions.

Three 10 m towers were constructed in the field. Their arrangement is shown in Figure 2. Three small platforms were mounted on each tower at 0.70, 3.56 and 9.56 m height. Turbulent velocity fluctuations were measured with one 3-component sonic anemometer and one 1-component sonic anemometer, both manufactured by Kaijō - Denki Co., Tokijō, Japan. Temperature fluctuations were obtained with two 10  $\mu$ m copper-constantan thermocouples. Static pressure fluctuations were measured with two probes, designed by Elliott (1972a). The thermocouples and pressure probes were built at the workshop. Inclinometers (Kaijō Denki) were used to record the tilt angle of the experimental set up. A close-up of the instrumentation, as it was usually installed on the platforms, is shown in Figure 3.

The frequency response of the measurement equipment was such that frequencies in the range from about 0.001 to 1 Hz could be detected. Throughout the experiment, meteorological data, such as the mean wind velocity, air temperature, air pressure and other weather data were provided by the weather station at the site. Finally, the various components of the surface energy balance were constantly monitored.

## 2.2 Data acquisition and processing

The signals from the instruments, installed in the field, were converted into direct currents before they were transmitted over a distance of about 100 m to a data-logging system. This data-logging system consisted of a LSI-11/03 mini computer and a CAMAC interface system. There the signals were transformed into volta-

ges and conditioned by means of amplifiers and filters. The signals were then fed to a 16-channel analog input board. Digital data acquisition was accomplished by sampling each of the 16 channels by means of a computer program in accordance with the sensor inventory. The data were stored on floppy-disk. After a measurement run had been completed, the data were copied to magnetic tape. The data were further processed by a PDP 11/34 computer at the laboratory and a Burroughs 7700 computer at the Technical University of Eindhoven (THE).

Airborne thermal infrared pictures of the experimental site were taken by Eurosense b.v., independently of the present experiments, from a height of about 550 m with a Daedalus DS 1240/1260 digital multispectral scanner with a MCT thermal infrared detector (channel 12 : 8-14  $\mu\text{m}$ ). Infrared line scanning (IRLS) provides pictures which contain information on the average temperature of a thin layer of air close to the surface.

### 2.3 Selection and description of the data

The active experimental period extended from 28 April to 9 May 1983. In choosing the data sets to be examined, it was decided to concentrate on those days when wind conditions were steady and when there was no cloud cover or complete cloudyness, so that shadows could not disturb the surface conditions. No data were obtained when the mean wind directions were within the sector from about  $190^\circ$  to  $210^\circ$ , as is shown in Figure 2. This sector was excluded because the nearby upwind terrain was not completely homogeneous in that direction due to some farms and sheds.

Each run contained about 20 minutes of data collection and was taken around midday. The midday structure of the PBL under convective conditions can be treated as if being in a steady state, because the time scale of convectively driven turbulence is much smaller than the time scale of changes in surface heat flux and the lowest inversion height, or changes in the pressure field that drives the flow (Kaimal et al., 1976). All data have been

corrected for tilt angles, as measured by the inclinometers, and they were detrended by applying a linear trend removal method. The thermal stability conditions were between unstable and neutral, excluding stable conditions.

Table I contains a general description of the data.

Table I. Description of data at the LHW site  
(for legend see next page)

Run	date	time (GMT)	$f_s$ ( $s^{-1}$ )	N	L(m)	tower	$z_1$ (m)	$z$ (m)	$\bar{u}_z$ ( $ms^{-1}$ )	$\bar{\phi}_z$ (deg)	$\bar{T}_z$ ( $^{\circ}C$ )
TJ8	7/8/81	1000			-7 <sup>b</sup>		800 <sup>d</sup>			70	
LA28	4/28/83	1509-1520	12.5	8275	-422 <sup>a</sup>	A	880 <sup>c</sup>	3.56	5.8	217	11.7
						A		9.56	6.7		11.4
IM4A	5/4/83	1347-1403	8.33	8275	-28 <sup>a</sup>	A	2000 <sup>d</sup>	0.70	2.9 <sup>e</sup>	320	12.4
						A		3.56	4.2		11.7
						C		0.70	2.9 <sup>e</sup>		12.4
						C		3.56	4.2		11.7
IM4B	5/4/83	1419-1436	8.33	8275	-35 <sup>a</sup>	A	2000 <sup>d</sup>	0.70	3.0 <sup>e</sup>	320	12.0
						A		3.56	4.4		11.6
						C		0.70	3.0 <sup>e</sup>		12.0
						C		3.56	4.4		11.6
IM9A	5/9/83	1055-1112	8.33	8275	-98 <sup>a</sup>	A	1090 <sup>c</sup>	0.70	4.2 <sup>e</sup>	220	12.2
						A		3.56	6.5		12.0
						B		0.70	4.2 <sup>e</sup>		12.2
						B		3.56	6.5		12.0
IM9B	5/9/83	1118-1140	6.25	8275	-62 <sup>a</sup>	A	1090 <sup>c</sup>	0.70	2.9 <sup>e</sup>	220	13.0
						A		3.56	5.0		12.8
						B		0.70	2.9 <sup>e</sup>		13.0
						B		3.56	5.0		12.8

(legend of Table I)

Run designation of the analyzed data. Values of the sampling rate ( $f_s$ ), the number of samples ( $N$ ), the Obukhov length ( $L$ ), the inversion height ( $z_i$ ), the measuring height ( $z$ ), mean wind velocity ( $\bar{U}_z$ ), the mean azimuth angle ( $\bar{\phi}_z$ ) and the mean temperature ( $\bar{T}_z$ ) are listed.

The surface roughness length, as obtained by assuming a logarithmic wind profile for high velocities at near neutral thermal stability conditions, was 22 mm.

Notes:

$L = -u_*^3 / (\text{kg } \overline{w'T'}/\bar{T})$  has been computed by

- a) the use of data of turbulence measurements, or
- b) the use of meteorological data and the various components of the surface energy balance and assuming a value of 2/3 for the Bowen ratio.

The lowest inversion height has been

- c) estimated from  $z_i \approx 0.25u_* / 1.1 \cdot 10^{-4}$  (Tennekes, 1970), or
- d) computed by using a simplified inversion rise model (Tennekes, 1973).

In this model  $z_i$  is estimated assuming that the inversion base generally grows linearly with time in the morning, and is proportional to the square root of time in the afternoon, before it reaches its maximum value. The maximum value has been taken as that observed at the meteorological site of the Royal Netherlands Meteorological Institute (KNMI), located near Cabauw at about 90 km to the south-west of the LHW site (cf. Figure 1).

- e) Value estimated from a value at another height, assuming the logarithmic law.

### 3. Experimental results

The turbulent structures have been detected by the VITA (variable interval time averaging) method (Chen and Blackwelder, 1978). The VITA method uses two parameters, viz. a short averaging time and a threshold level. The short averaging time corresponds to the timescale ( $\tau$ ) of the turbulent structures. This timescale is defined as twice the width of the sharp upstream edge of the characteristic asymmetric triangular patterns in the temperature record. The square root of the threshold level ( $k$ ) is a measure for the amplitude, or strength, of the sharp interface of the characteristic patterns inside the turbulent structures (Schols, 1984).

It is impossible to define one unique timescale or frequency of occurrence and amplitude scale of the turbulent structures. Using the VITA method information is obtained on the timescale distribution and the amplitude distribution of the structures in the ASL.

Figure 4.a shows the distribution of the timescale of the turbulent structures for different values of the threshold level. Figure 4.b shows the distribution of the amplitude of the turbulent structures for different values of their timescale.

The fractional number of turbulent structures, as detected by the VITA technique, is an estimate of a two-dimensional probability distribution based on the timescales and amplitudes of the turbulent structures. The probability distribution can be used to compute the average values of the short averaging time and the threshold level. Both sets of graphs in Figure 4 show common characteristics: As the mean amplitude of the turbulent structures grows, their average timescale grows too.

Once a reference point in time for each turbulent structure has been determined, it is possible to study the structure in time and space by performing a conditional averaging procedure. This means that ensemble averages of the turbulent signals are compu-

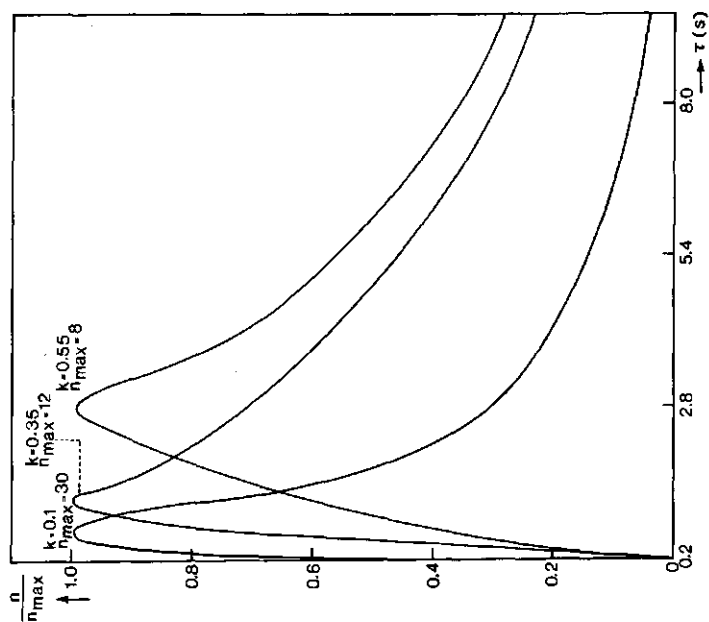


Figure 4.a The number ( $n$ ) of turbulent structures, as a fraction of its peak value ( $n_{\max}$ ), versus their time scale ( $\tau$ ). The graphs have been drawn for different values of the threshold level ( $k$ ). Data are from Run LA 28.

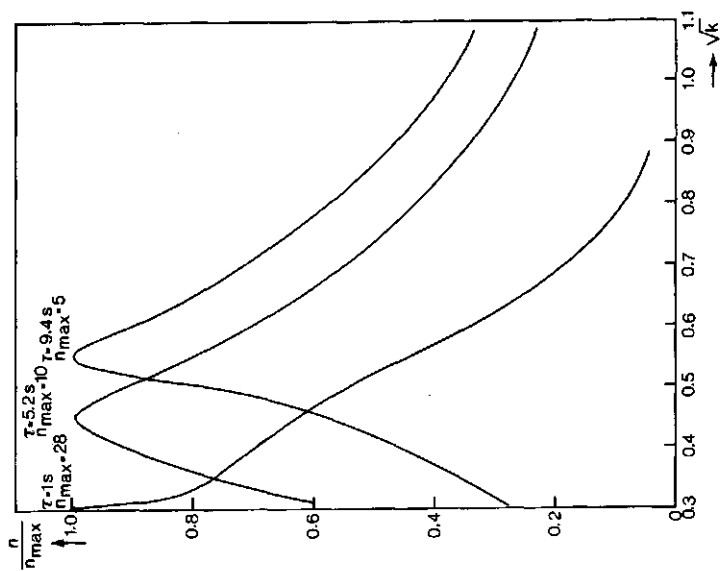


Figure 4.b The number ( $n$ ) of turbulent structures, as a fraction of its peak value ( $n_{\max}$ ), versus the square root of the threshold level ( $k$ ). The graphs have been drawn for different values of the time scale ( $\tau$ ) of the turbulent structures. Data are from Run LA 28.

ted around the time that a turbulent structure has been detected. The relationship of the turbulent structures to their environment is expressed in terms of their temporal behavior and spatial distribution. The temporal behavior includes translation speed, lifetime of the turbulent structures, etc. The spatial distribution includes horizontal distribution and inclination angle to the surface of the sharp upstream edge of the turbulent structures. The quantitative behavior of the turbulent structures, as detected by the VITA method, depends on their timescale and the threshold level. The present paper contains a description of the properties of mainly those turbulent structures which contribute most significantly to the turbulent vertical transports of momentum and heat.

### 3.1 Contribution of turbulent structures to turbulent vertical transports

The contributions of the ensemble-averaged turbulent structures to the mean value of the turbulent vertical transports of horizontal alongwind momentum and heat have been computed for time intervals of about four times the time scale of the turbulent structures. The mid-point of such a time interval was taken at the sharp upstream temperature interface of the turbulent structures. The ensemble-averaged contributions of the turbulent structures to the turbulent transports are maximal at the average values of the threshold level and the time scale of the structures, as computed using the aforementioned two-dimensional probability distribution.

Table II contains a general summary of the results obtained at a height of 3.56 m. These data show that during 15 to 20 percent of the total observation time between 30 and 50 percent of the turbulent momentum transport and between 40 and 50 percent of the turbulent heat flux is produced inside the turbulent structures which are most significant of the turbulent transport process.

Table II. Contribution to turbulent transports

Percentage contribution of the ensemble-averaged turbulent structures to the turbulent vertical kinematic transports of horizontal alongwind momentum ( $p_{u,w}$ ) and heat ( $p_{w,T}$ ) measured at a height of 3.56 m. The time fraction ( $\gamma$ ), during which these contributions take place, has also been presented.  $n$  is the number of processed turbulent structures.  $k_{ave}$  denotes the average value of the threshold level, which has been computed using the two-dimensional probability distribution referred to in the text.  $\tau_{ave}$  is the average value of the time scale of the turbulent structures, which has been obtained in the same way.

Run	duration (s)	n	$\tau_{ave}$ (s)	$k_{ave}$	$\gamma$	$P_{u,w}$ (%)	$P_{w,T}$ (%)
LA28	662	7	5.2	0.35	0.15	30	51
LM4A	993	12	6.4	0.52	0.21	43	44
LM4B	993	11	5.7	0.53	0.19	45	47
LM9A	993	15	6.2	0.48	0.23	52	53
LM9B	1324	20	6.0	0.44	0.20	38	42

### 3.2 Temporal behavior

The turbulent structures are assumed to propagate along the mean wind direction in the ASL. Turbulence signals obtained from sensors, which are separated in the direction of the mean wind have been processed to obtain information about the temporal behavior of the turbulent structures.

#### 3.2.1 Translation speed

The translation speed of the turbulent structures was obtained by computing the cross correlation function between two registrations of a single turbulent signal measured at horizontally separated locations. The time delay at which the cross correlation has its maximum value is the transit time of the bulk of turbu-

lent structures which advect between the two locations. The translation speed ( $U_c$ ) of the structures in the ASL is then computed by the separation in the direction of the mean wind, between the locations, divided by the transit time. The results of the calculations of  $U_c$  for the temperature, horizontal alongwind velocity and static pressure signals yield about the same value with an uncertainty of about 10%. The magnitude of this uncertainty was obtained from the difference between the estimates of  $U_c$  between the various tower combinations. The value of  $U_c$  amounts about fifteen times the surface friction velocity for the present data here. This value, which is in close agreement with the value found by Kaimal (1974), corresponds to the value of the horizontal wind speed averaged over the depth of the ASL (see appendix A).

The cross correlation technique may well weight large scale turbulent structures other than smaller scale structures. To obtain the advection speed of individual frequency bands, or scales of turbulent structures, the coherence and phase spectra between two registrations of a single turbulent signal are analyzed. The advection speed is computed as the phase speed ( $U_p$ ), which is obtained by using the phase angle ( $\phi$ ) of the cross spectral density function. This is given by

$$\phi = \tan^{-1}(Q/Co) \quad , \quad (3.1)$$

where  $Q$  and  $Co$  are the quadrature spectrum and the Co-spectrum, respectively. Both spectra, together, constitute the cross-spectral density function  $G$ . This function may be written as  $G = Co - jQ$ , where  $j$  is the imaginary unit. When turbulence is advected downwind in a frozen pattern, the phase angle between large scales is given by

$$\phi = - 2\pi fl/U_p \quad , \quad (3.2)$$

where  $l$  is the downwind separation of the sensors, and  $f$  denotes the frequency. The range of scales for which the turbulence is

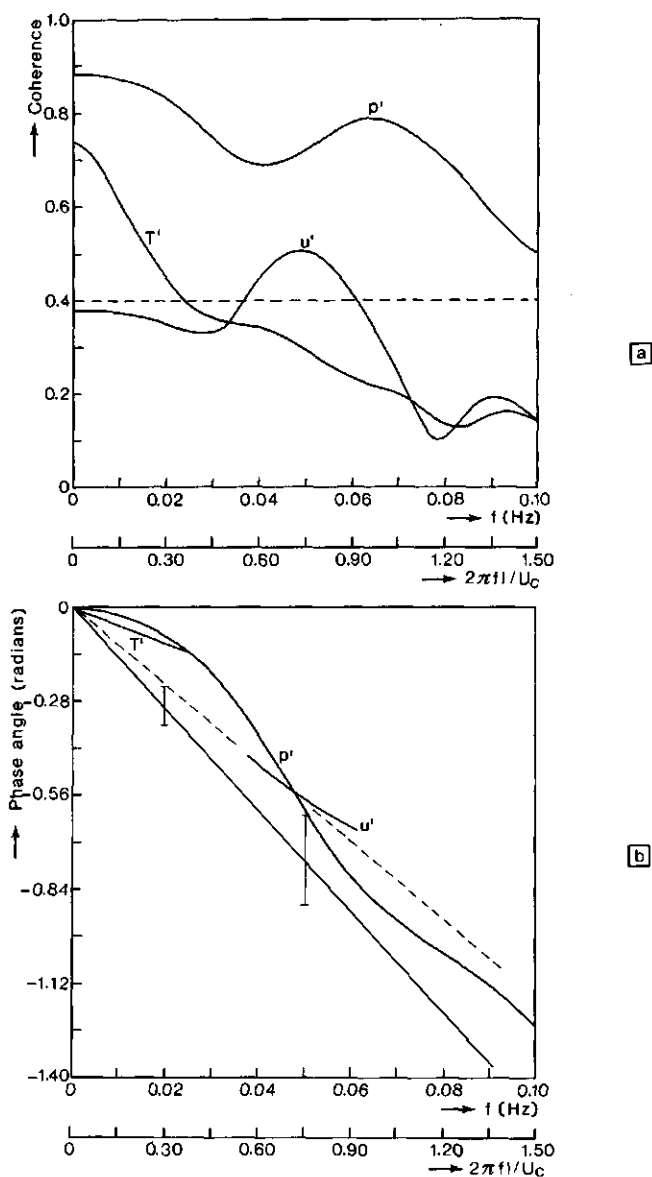


Figure 5 Coherence characteristics and phase angle distribution of turbulent signals of temperature ( $T'$ ), horizontal alongwind velocity ( $u'$ ) and static pressure ( $p'$ ) from Run LM 9. The straight line piece in the phase diagram is obtained when the phase speed ( $U_p$ ) is equal to the translation speed ( $U_c$ ) computed using the cross correlation technique. The uncertainty limits for  $U_c$  are indicated by vertical bars.

advected in a frozen pattern can be found by studying the coherence function. The coherence function is a measure, in the frequency domain, of the correlation between two registrations of a turbulent signal, irrespective of their phase shift. The coherence function (Coh) is averaged over a small frequency band and is given by

$$\text{Coh} = \left\{ \frac{C_o^2 + Q^2}{G_1 G_2} \right\}^{\frac{1}{2}} \quad (3.3)$$

where  $G_1$  and  $G_2$  are the power spectral densities of the respective registrations. The coherence function has a maximum value of unity and a minimum of zero. The assumption of 'frozen pattern' advection is accepted when the coherence function exceeds some predefined value.

Figure 5.b shows the phase angle distributions for the turbulent signals of temperature, horizontal alongwind velocity and static pressure from Run LM 9. The phase angles have only been plotted in the frequency range where the coherence function, as shown in Figure 5.a, has a magnitude larger than 0.4. The straight line in Figure 5.b is obtained when the phase speed is equal to the translation speed as computed by the cross correlation technique. The phase diagrams all show a phase speed which is larger than the translation speed. This trend may be partly due to the turbulent variability in the direction of the mean wind (Wilczak and Tillman, 1980). Any turbulent fluctuation in the mean wind direction, with a timescale of the order of the time some turbulence scale needs to travel from one sensor to another, will result in an overestimate of the phase speed of that scale.

In Figure 6 this effect is illustrated: For a turbulent structure, which is advected at an angle  $\theta'$  to the mean wind, the phase difference between the locations A and B is computed a factor  $\cos\theta'$  too small, since that structure is assumed to travel along the mean wind direction. The phase speed is thus overestimated by a factor of  $1/\cos\theta'$ .

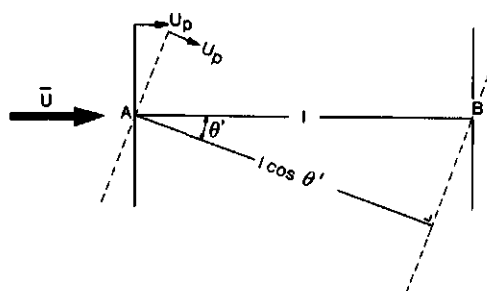


Figure 6 Schematic of orientation of two sensors A and B, mean wind direction and wind direction fluctuation  $\theta'$ . The vertical solid lines and the broken lines represent phase fronts, i.e. lines which connect points of equal phase.

The broken line piece in Figure 5.b is the phase diagram for a turbulence field which propagates at a translation speed closely corresponding to the phase speed, averaged in the frequency domain, emerging from the phase diagram of the static pressure signal. There is a most significant discrepancy at the lowest frequencies ( $f < 0.03$  Hz) between the broken line piece and the phase diagrams of the static pressure signal and the temperature signal. In this frequency range, the phase speed of the static pressure field and the temperature field is about twice the value for the static pressure field at higher frequencies ( $f > 0.06$  Hz).

### 3.2.2 Lifetime

The turbulent structures in the ASL maintain their distinct identity and propagate coherently for only a limited distance. The turbulent structures deteriorate as they advect downstream.

Figure 7 presents the ensemble-averaged turbulent structures of Run LM 4A. The characteristic jumps in the patterns of turbulent temperature and horizontal alongwind velocity measured at the upstream location (tower A) is seen to have almost been disappeared at the downstream location (tower C). The pulse shaped turbulent static pressure pattern around  $t = 0$  keeps its identity more

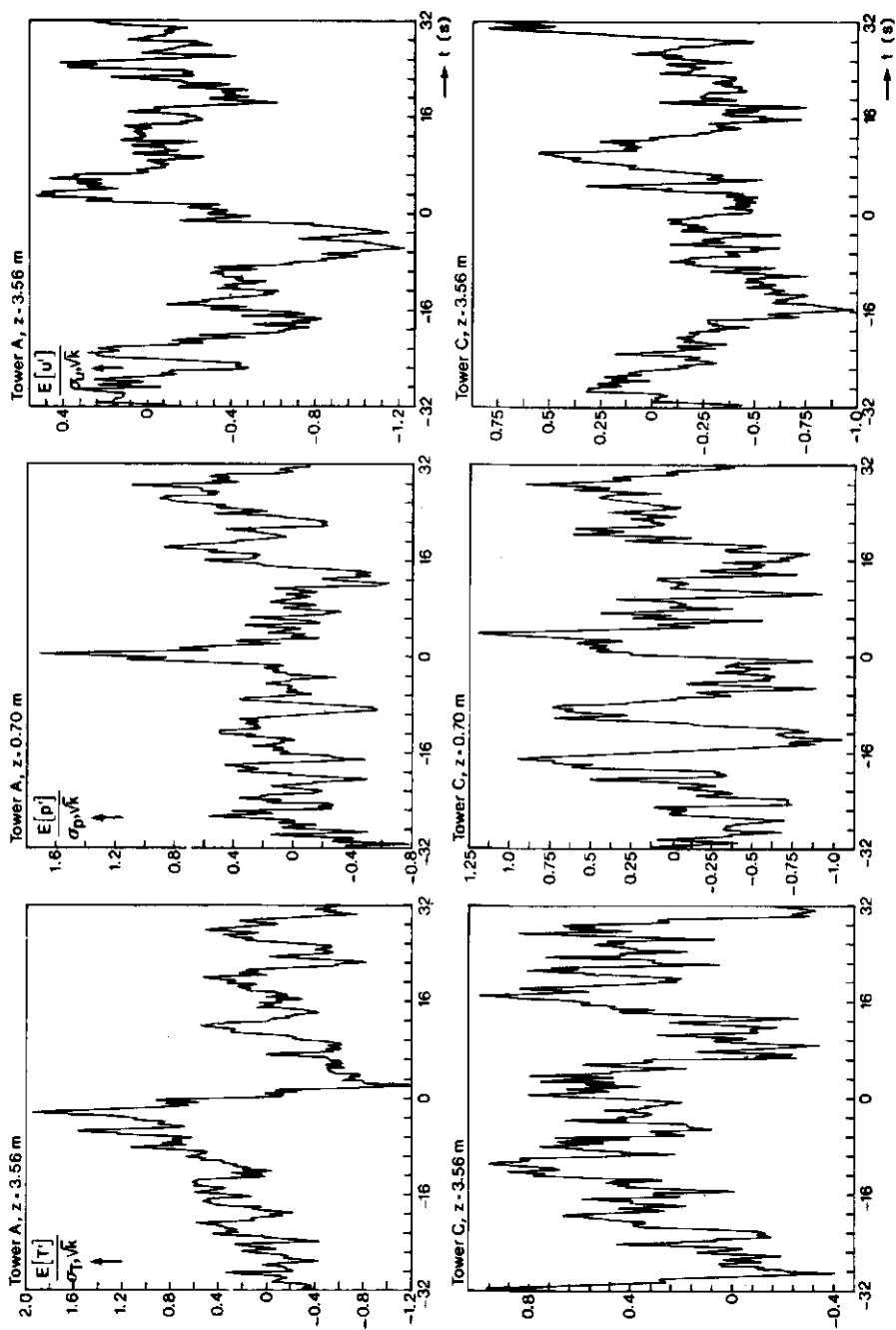


Figure 7 Ensemble-averaged turbulent signals of Run LM4A. The temperature signal at the upstream tower (A) has been taken as detection signal for the turbulent structures ( $n = 12$ ,  $\tau = 6.4$  s,  $k = 0.52$ ).

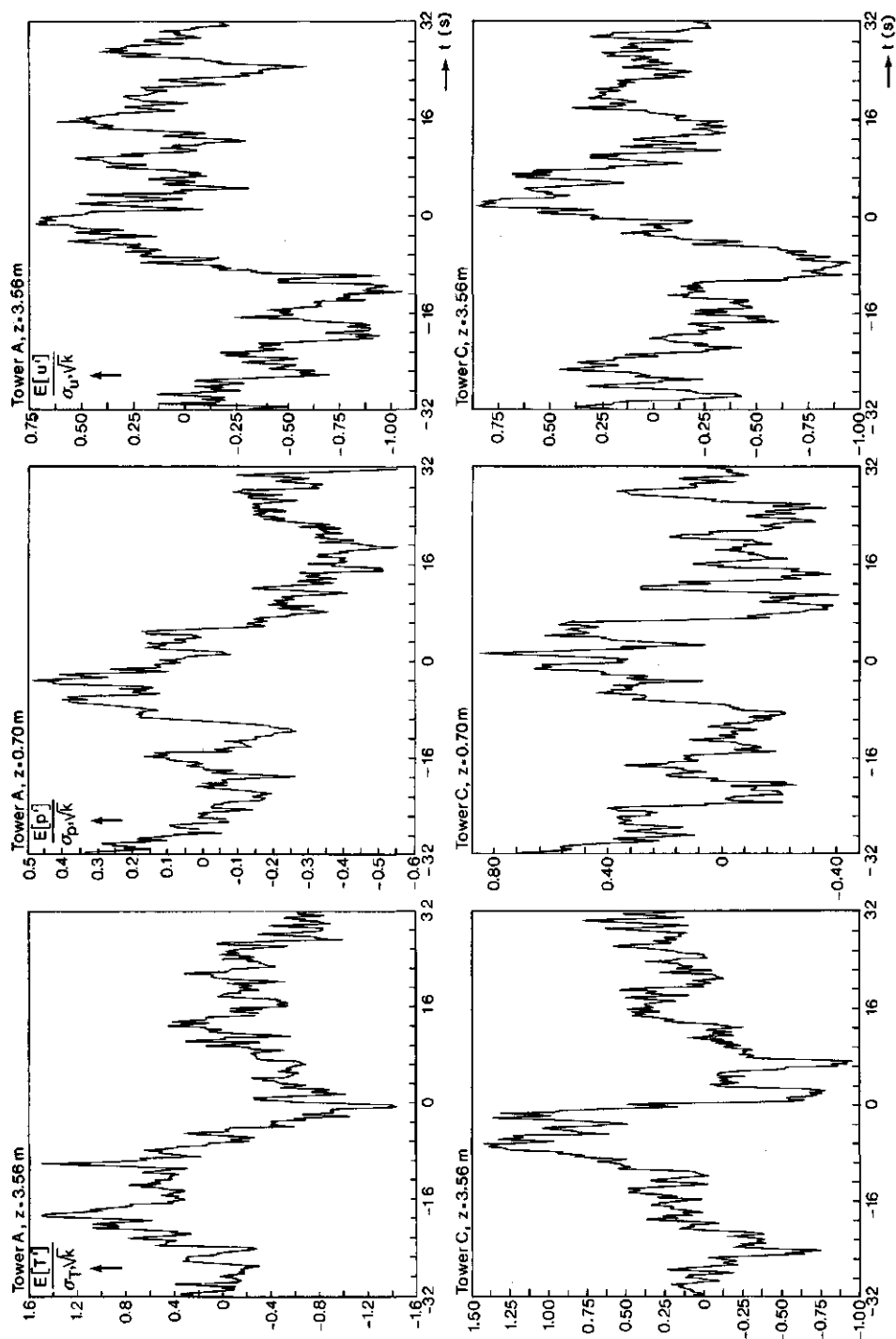


Figure 8 Ensemble-averaged turbulent signals of Run LM4A. The temperature at the downstream tower (C) has been taken as detection signal for the turbulent structures.

clearly as it advects downstream.

The distortion of the characteristic patterns in the turbulent structures as they travel downstream is caused by several reasons: First, the three-dimensional character of the turbulent structures makes them pass the sensors at different spanwise locations. Therefore, the size of the individual members of the ensemble averages varies from one realization to another. Second, the phase speed of each turbulent structure varies from one to another. This introduces a random phase into the ensemble-averaged turbulent signals, the so-called 'phase jitter'. Third, the turbulent structures degrade due to the strong nonlinear interactions present in turbulent flows and they finally dissipate into eddies of the smallest scales.

Figure 8 again shows the ensemble-averaged turbulent signals of Run LM4A. The downstream temperature signal has been taken as the detection signal for the turbulent structures. The discrepancy between the upstream patterns and those downstream is much less pronounced than in Figure 7, where the upstream temperature signal had been used as detection signal for the turbulent structures. It is evident from comparison of these two sets of graphs that the nonlinear interactions between turbulent structures of varying scales and strength contribute most significantly to the deterioration of their ensemble averages as they propagate downstream. The pulse shaped pressure patterns inside the turbulent structures are the least distorted and they have the highest coherence level (cf. Figure 5.a).

The static pressure fluctuations are an integral result of the turbulent velocity fluctuations in their neighborhood. The characteristic static pressure patterns inside the ensemble-averaged turbulent structures are caused by sharp jumps in the wind velocity of various scales and strength in their vicinity. Although the ensemble-averaged velocity patterns may lose their identity, the static pressure patterns are more persistent as they propagate through the turbulence field.

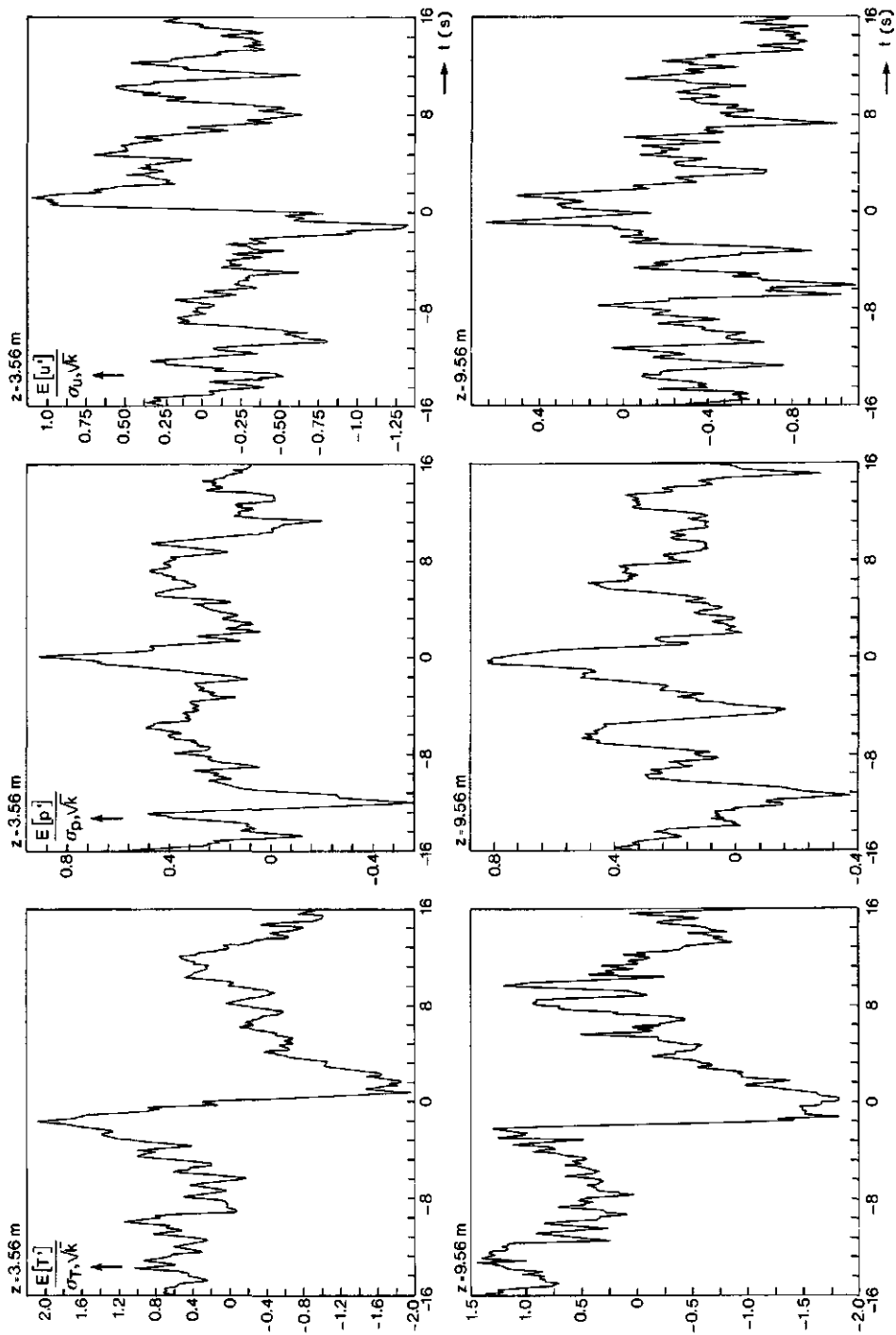


Figure 9 Ensemble-averaged turbulent signals of Run LA28. The temperature signal at 3.56 m height has been taken as detection signal for the turbulent structures ( $n=7$ ,  $\tau=5.2s$ ,  $k=0.35$ ).

### 3.3 Spatial distribution

The spatial properties of the turbulent structures depend on their translation velocity, which is found to be about the horizontal wind velocity averaged over the depth of the ASL.

#### 3.3.1 Inclination angle

The inclination angle of the turbulent structures measured from the surface, is computed by using the time difference between the passing of the upwind edge of the turbulent structures at vertically separated locations on a tower and the translation speed.

Figure 9 presents the ensemble-averaged turbulent structures of Run LA28. There exist definite time delays between both temperature patterns and both velocity patterns at the two height levels, while between the pulse shaped static pressure patterns hardly any time shift is discernable. The cross correlation technique and the phase method both yield about the same results. The inclination angle of the temperature interface is about  $40^\circ$ , that of the internal shear layer, as determined by the velocity interface amounts to  $60^\circ$ , while the static pressure patterns move on a line almost perpendicular to the surface. This result is made plausible when the scale of the turbulence field which contains the temperature interface is considered to be larger than that which contains the velocity interface near the surface, and the static pressure patterns are considered to be caused mainly by velocity fluctuations in a narrow layer near the surface.

#### 3.3.2 Horizontal distribution

IRLS pictures of the experimental site were taken around 10 GMT on 8 July 1981. The thermographic image presented in Figure 10 shows wind patterns, which consist of more or less parallel boundaries of lighter and darker tones in the direction of the mean wind. These bands of 'striae' are not related to objects, like

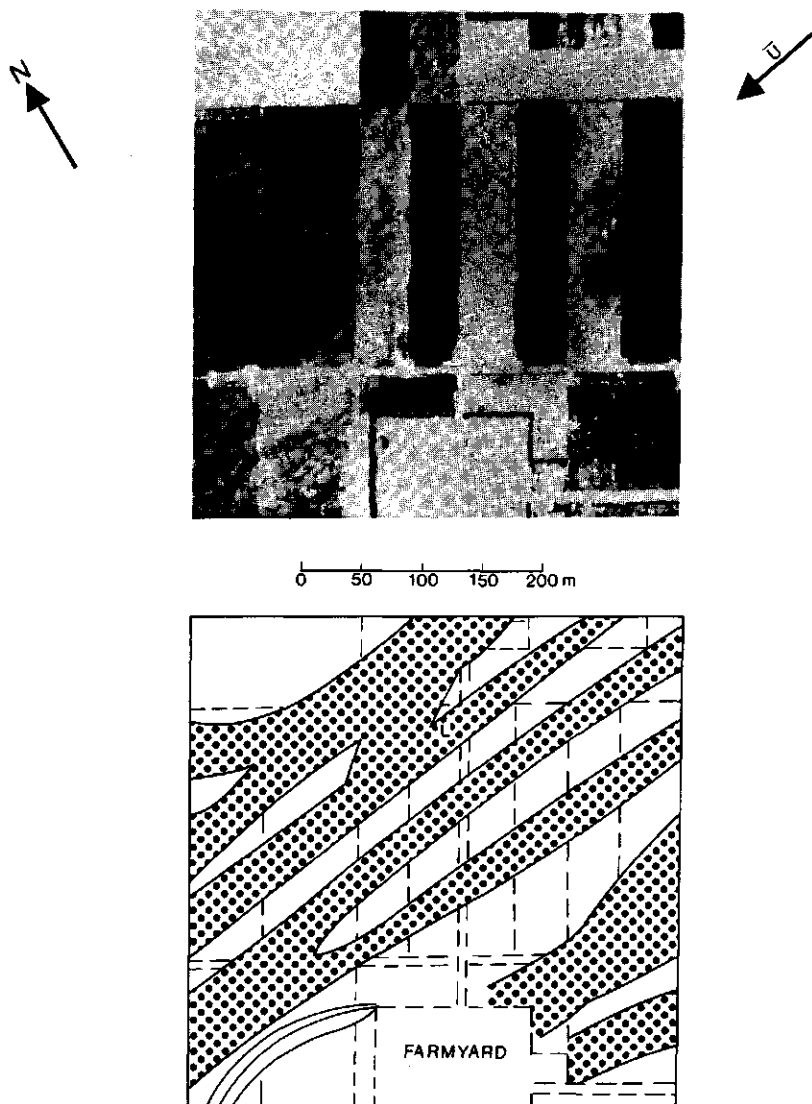


Figure 10 Thermographic image of the experimental site. The lower picture shows the bands (shaded) of relatively warm air, which are parallel to the mean wind. The rectangular light and dark areas in the upper picture respectively represent pastures which have recently been mowed or not. The image has been scanned within approximately 7 s. For further description see text.

trees, or houses that mark their upwind end, as is verified by thermographic images taken of the same area with short time intervals, when the 'striae' appear at different places.

The wind patterns have also been observed by other investigators (Derksen, 1974) and they have been related to air parcels with different temperatures close to the surface. The range of temperatures scanned by the infrared detector was between 20.5°C and 26.8°C, while its resolution was 0.125°C. The mean air temperature at 10 cm height was 26.6°C. The lapse rate through the depth of the PBL was about 0.01°C/m, as observed at the meteorological site of the Royal Netherlands Meteorological Institute (KNMI), located near Cabauw about 90 km to the south-west of the LHW site (cf. Figure 1). The temperature difference between the cold and warm bands of 'striae' is estimated to be about 2°C. The cold air masses thus must come from a height of about 200 m.

The wind patterns in Figure 10 are about 50 m wide and extend in the wind direction along the entire length of the picture, which amounts to several hundreds of metres. The wind patterns are considered to be the result of the existence of turbulent structures. The bands of dark 'striae' correspond to descending cold air masses moving at a higher speed than the average wind speed near the surface. The bands of lighter 'striae' refer to ascending low speed air masses. The vertical extent of the wind patterns is of the order of the depth of the ASL, as inferred from the magnitude of the temperature difference between the adjacent bands of light and dark 'striae' and the magnitude of the lapse rate. In this respect one may think of the thermal sheets postulated by Priestley (1959).

#### 4. Formation mechanism

The concept of vorticity is used to explain the formation of the wind patterns as observed in Figure 10. The warm patches correspond to convergence zones between counterrotating streamwise vortices, as is shown in Figure 11. In this respect we may think of

the horizontal rolls suggested by Businger et al. (1967). These vortices are the result of a secondary instability mechanism, which refers to a possible generation of a secondary flow over and above the flow that is already present. A secondary flow is one in which there is a vorticity component aligned in the same direction as the mean flow.

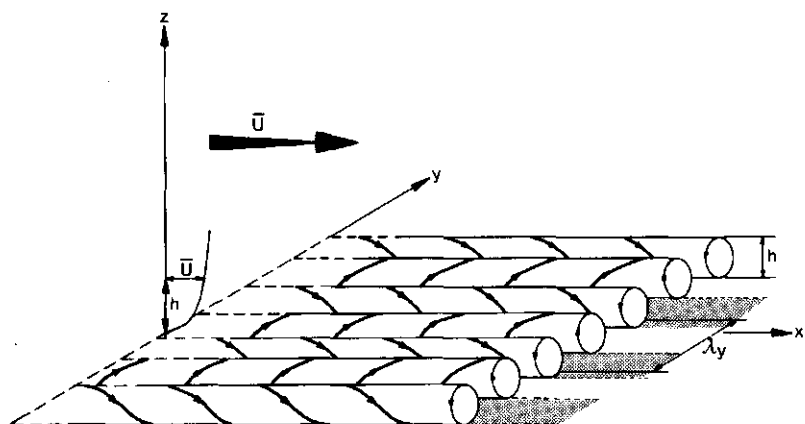


Figure 11 Longitudinal convection cells producing convergence zones (shaded) with an average lateral spacing ( $\lambda_y$ ) of  $2 h\sqrt{2}$ .  $h$  is the average diameter of the cells.

The curvature of the vertical profile of mean horizontal velocity in the ASL enforces alignment of convective cells with the flow direction (see appendix B). The dimensions of the longitudinal rolls are mainly regulated by such factors as the surface friction velocity ( $u_*$ ) and the scaling temperature ( $T_*$ ), as expressed by Equation (B.4).

For the data of Figure 10, the values of  $u_*$  and  $T_*$  were  $0.26 \text{ ms}^{-1}$  and  $-0.7^\circ\text{C}$  respectively. This results in an average cell diameter of 25 m and a mean lateral spacing between the convergence zones of about 70 m as can be established from the wind patterns in Figure 10.

## 5. Conclusions

Turbulent structures in the ASL contribute to a large part of the turbulent transports of momentum and heat. The bulk of these turbulent structures travels at a velocity  $U_c$  which is identified with the horizontal wind velocity averaged over the depth of the ASL. The phase speed of the individual scales of the static pressure field decreases from about twice  $U_c$  at low frequencies to a value a little lower than  $U_c$  at higher frequencies. The pressure fluctuations at the low frequencies are caused by the passage of convective elements which contain air lighter than their surroundings. At higher frequencies, the pressure fluctuations are an integral result of the turbulent velocity fluctuations.

The sharp upstream temperature interface inside the turbulent structures is inclined to the surface at an angle smaller than the internal shear layer. This finding indicates that the scale of the turbulence field which contains the temperature interface is larger than that which contains the internal shear layer close to the surface. The large scale temperature interface travels from greater heights to the surface, which can be verified by inspection of IRLS pictures (cf. Figure 10) of the measuring site: The temperature difference between the warm air in the convergence zones and that outside equals the difference between the mean temperature of the air close to the surface and that at a height of a few hundreds of metres.

The wind patterns, as shown by such thermographic images are the result of the existence of turbulent structures. IRLS pictures therefore provide a snap shot image of the instantaneous horizontal distribution of the turbulent structures. The turbulent structures are the result of the formation of longitudinal convection cells in the unstable ASL (cf. Figure 11). The diameter of these rolls scales on the ASL parameters  $u_*$  and  $T_*$ . The light bands of 'striae' in Figure 10 refer to ascending relatively warm air masses of relatively low speed inside convergence zones between counterrotating rolls along the mean wind direction. The

dark bands along the mean wind direction are connected to descending relatively cold and high speed air masses. The boundaries between the dark and light bands correspond to the sharp temperature interfaces inside the turbulent structures.

The convergence zones extend to several hundreds of metres in the direction of the mean wind and they may thus move over one and the same point for a considerable time. The turbulent transports in the convergence zones are much larger than outside. It is therefore necessary that, in order to obtain good estimates of the mean values of the turbulent transports, point measurements of these quantities have to be averaged over a sufficient long time interval. When this is impossible, due to e.g. non-stationarity of the turbulent field, the point observations may give questionable results, as Businger et al. (1967) have already pointed out.

The turbulent structures in the ASL are short living appearances due to the strong nonlinear interactions between the various scales of turbulence. The static pressure patterns inside the turbulent structures maintain their identity most clearly, since they represent an integral result of the sharp velocity interfaces of various scales in their vicinity.

The role of the static pressure fluctuations inside the turbulent structures will be described in a forthcoming paper. Special attention will be paid to the spatial gradient of static pressure within the turbulent structures. Further, knowledge of the role of the pressure-velocity gradient interactions in the turbulent mechanical energy transfer, between the three velocity components, will provide more insight in the dynamical properties of the turbulent structures.

#### IV. A dynamical description of the turbulent structures in the near neutral atmospheric surface layer: The role of static pressure fluctuations \*

**Abstract** Turbulent structures in the near neutral atmospheric surface layer (ASL) contain two distinct time scales: A sharp small scale fluctuation is superimposed on a large scale variation. The small scale fluctuation can be recognized as a pulse shaped pattern in the turbulent static pressure signal. This pulse is caused by the sharp downward fluctuation of vertical velocity, which is associated with the internal shear layer at the upstream back of the turbulent structure. The large scale variations of the static pressure are caused by the passage of convective elements, which contain air lighter than their surroundings.

The turbulent static pressure fluctuations transfer mechanical turbulent energy in two different ways: First, the static pressure-vertical velocity correlation term feeds kinetic energy at the low frequency end of the region of appreciable turbulent shear stress into the vertical velocity fluctuations. Second, the static pressure-horizontal velocity gradient interactions extract turbulent mechanical energy from the horizontal alongwind velocity fluctuations at the high frequency end of the region of active turbulent shear stress. This energy is mainly redistributed to the vertical velocity fluctuations.

Inside an average turbulent structure, just downstream of its sharp upstream interface, the low-speed fluid is ejected due to a turbulent vertical static pressure gradient force. The vertical gradient of the turbulent static pressure provides the link between the small scale and large scale organized motions inside the turbulent structures in the ASL.

\*Submitted to Boundary-Layer Meteorology with L. Wartena as co-author.

## 1. Introduction

The static pressure fluctuations play a crucial role in the description of the dynamical behavior of the turbulent structures in the ASL, as defined in a recent paper (Schols, 1984). The static pressure field can roughly be divided into two scale regions. The properties of the static pressure variations have been investigated for each of these scale regions.

Section 2 contains a brief description of the static pressure sensors used in the present investigation. The dynamical properties of the turbulent structures in a near neutral ASL are described in Section 3. The pressure velocity (gradient) interactions in the budget of mechanical turbulent energy have been measured for the horizontal alongwind velocity component and the vertical velocity.

In Section 4 a description is presented on the role of static pressure fluctuations in the mechanism of origin and development of the turbulent structures in the ASL. Special attention has been paid to the spatial static pressure gradients inside the turbulent structures.

## 2. Pressure instrumentation

In order to measure the turbulent static pressure variations in the ASL two pressure sensors were built. The design of these instruments was similar to that described by Elliott (1972a), except for some modifications. As is shown in Figure 1, a sensor mainly consists of a probe (not visible) as described in Elliott (1972a) and a streamlined case containing a differential pressure transducer, DPT, (Validyne type DP 103) with a range of operation between  $-8.8$  and  $8.8$  mm H<sub>2</sub>O. The DPT has an accuracy of 0.5% of the full scale reading and a flat frequency response up to 1 kHz. The sensitivity and frequency response of the measuring device were chosen such that it operated optimally in the frequency range between 0.001 Hz and 1 Hz.

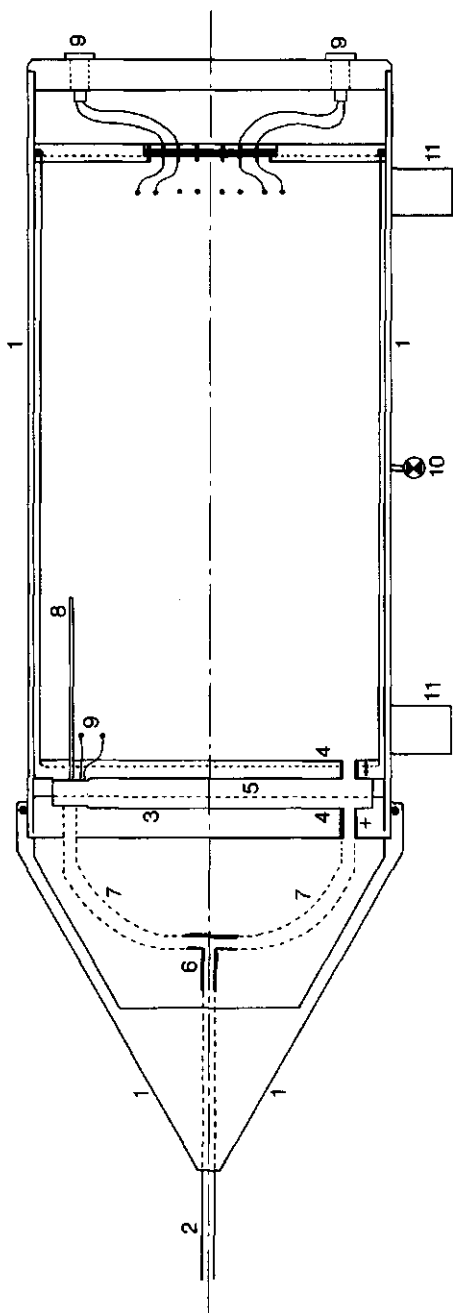


Figure 1 Static pressure sensor. Its constituents are indicated by numbers. 1. Streamlined glass wool-insulated case. 2. End of probe. 3. Differential pressure transducer. 4. Pressure ports. 5. Diaphragm. 6. Tee-piece. 7. Tubes. 8. Pneumatic restriction. 9. Electronic parts and connections. 10. Valve. 11. Standard-bearer.

An extensive calibration program, as described by Elliott (1972a), was performed in order to get data on the quality of the pressure sensors. In Figure 2 the filter response of a pressure sensor is shown. The high frequency part ( $0.05 < f < 1$  Hz) mainly represents the first order characteristics of the pressure probe. The drop-off at the low frequency end is mainly governed by the pneumatic restriction in the case. This sample is typical of those obtained for both sensors. The accuracy of the calibration is approximately 1% in the amplitude response and about  $5^\circ$  in the phase response, as is also indicated in Figure 2.

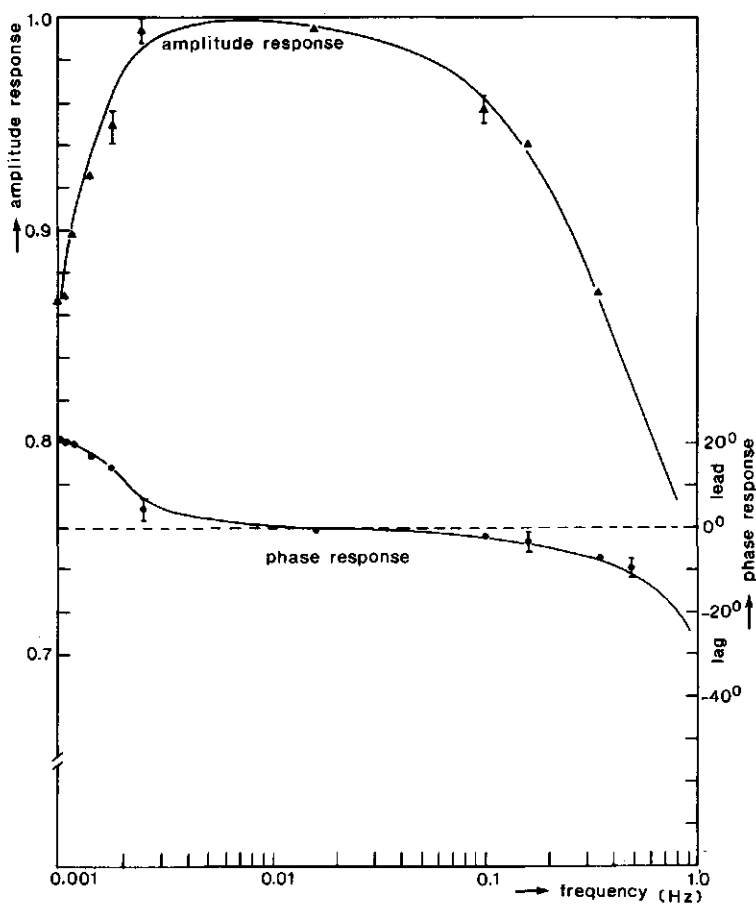


Figure 2 Filter response of a pressure sensor. The accuracy of the calibration is indicated by vertical bars in the graph.

When a static pressure sensor is exposed to an air flow, dynamic pressure fluctuations arise, which are generated by the interference between the flow field and the body of the probe. At a turbulence level of 25%, which is common in the ASL, the magnitude of the variations of the stagnation pressure is equal to about 30% of its value (see appendix C). The calibration results of the present probes here show a linear relationship between the level of the generated dynamic pressure fluctuations at the probe and the stagnation pressure. Besides, that level is smaller than 4% of the stagnation pressure. Therefore, the variation of the level of the dynamic pressure fluctuations amounts to one third of its value too, which is smaller than approximately 1% of the stagnation pressure.

It is assumed that the surface friction velocity is about 7% of the wind speed averaged over the depth of the ASL (see appendix C). The magnitude of the fluctuations of the turbulent static pressure is then about 3% of the stagnation pressure averaged over the depth of the ASL. The variation of the level of the generated dynamic pressure fluctuations at the probe is smaller than 1% of the stagnation pressure. The signal to noise ratio for the measurement of the static pressure fluctuations is better than 3:1. The pressure-velocity (gradient) terms can thus be measured to an accuracy of 30% for their amplitude and about 5% for their phase content.

### 3. Dynamics of turbulent structures

Beside the static pressure fluctuations, turbulent variations of wind velocity and air temperature have been measured. Details about the data acquisition procedure and processing can be found in a recent paper (Schols et al., 1984). Table I contains a description of the data which were obtained from a nearly neutral thermally stratified ASL. For the present investigation the turbulence data were high-pass filtered by differencing with respect to low-passed data. The filter effectively attenuated frequencies below 0.0015 Hz.

Table I. Description of the data

List of significant boundary-layer parameters and mean conditions under which the run mentioned in this report was taken. In an earlier report the run has been referred to as LA28 (Schols, 1984).

Surface roughness length $z_o$	=	0.022 m
Measuring height $z$	=	3.56 m
Obukhov length $L$	=	- 422 m
Lowest inversion height $z_i$	=	880 m
Mean wind velocity $\bar{U}_z$	=	5.8 $\text{ms}^{-1}$
Mean temperature $\bar{T}_z$	=	11.7° C
Standard deviations of turbulent variations	$\sigma_{u'}$	= 0.96 $\text{ms}^{-1}$
	$\sigma_{w'}$	= 0.40 $\text{ms}^{-1}$
	$\sigma_{T'}$	= 0.13° C
	$\sigma_{p'}$	= 0.63 $\text{Nm}^{-2}$
surface friction velocity $u_*$	=	0.39 $\text{ms}^{-1}$
surface scaling temperature $T_*$	=	- 0.026° C

### 3.1 Scale characteristics

Spectra of the turbulence data were computed using the fast-Fourier technique. Spectral forms involving the product with the frequency ( $f$ ) are referred to as logarithmic spectra. The peaks of the logarithmic spectra are most appropriate as indicators of the existing scales in the turbulence field (Zangvil, 1981).

Figure 3 shows the logarithmic spectra of the present turbulence data plotted against the frequency made dimensionless by using the Taylor hypothesis, i.e.  $\partial f / \partial x = -(1/\bar{U}) \partial f / \partial t$ . The spectra of static pressure ( $p'$ ), temperature ( $T'$ ) and horizontal alongwind velocity ( $u'$ ) show distinct peaks in both a low-frequency region (A) and a high-frequency region (B). The spectrum of vertical

velocity ( $w'$ ) has only one peak in the high-frequency region.

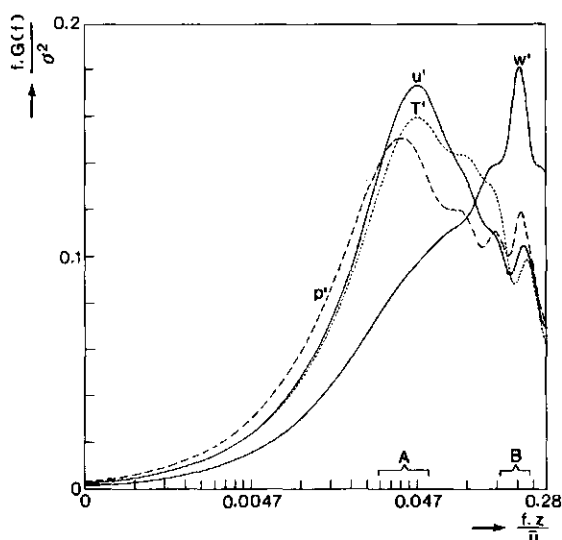


Figure 3 Logarithmic spectra of turbulent fluctuations of horizontal alongwind velocity ( $u'$ ), vertical velocity ( $w'$ ), air temperature ( $T'$ ) and static pressure ( $p'$ ), normalized by their respective variance, plotted against the dimensionless frequency.

Figure 4 presents the picture of an average turbulent structure, which can be recognized by the characteristic patterns occurring almost simultaneously in the various turbulence signals. The patterns of the  $T'$  and  $u'$  signals show two distinct timescales. A small one lies closely around  $t = 0$ , the reference time for the turbulent structure, and is characterized by a sharp fluctuation. This rapid intense variation is embedded in a large-scale motion around the reference time. The large timescale is about one order of magnitude larger than the small timescale. The two timescales correspond to the regions denoted by A and B on the frequency axis in Figure 3. The static pressure pattern also contains two dominant timescales of variation, while the vertical velocity pattern shows only one distinct small scale intense fluctuation at the upstream interface at  $t = 0$ .

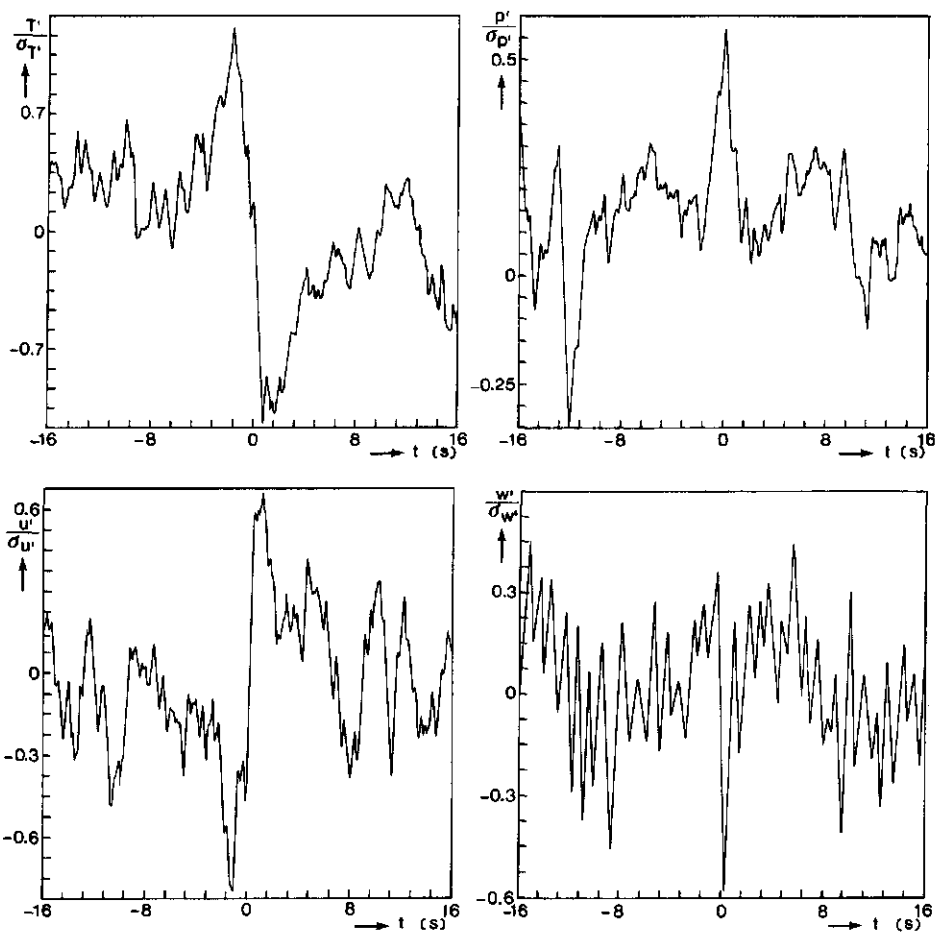


Figure 4 Patterns characteristic of an average turbulent structure. The signals have been smoothed by a moving average over 4 points.

The small scale fluctuations in the static pressure are the integral result of the turbulent velocity fluctuations in the ASL in the presence of a mean strain field. Thomas and Bull (1983) measured wall-pressure variations in a turbulent boundary layer. They showed that a vertical velocity pattern, such as that shown in Figure 4 produced a pulse shaped static pressure variation as IV.8

also shown in Figure 4.

The pulse shaped static pressure fluctuations are superimposed on large scale variations. These large scale variations of the static pressure are caused by the passage of convective elements which contain air lighter than their surroundings.

### 3.2 Static pressure-velocity (gradient) relationships

The static pressure fluctuations contribute to the transfer of turbulent mechanical energy in two different ways: First, the height-integrated total turbulent kinetic energy budget contains a static pressure-vertical velocity correlation term ( $-p'w'$ ). Second, the turbulent kinetic energy is transferred between the three velocity components by means of static pressure-velocity gradient interactions (see Appendix D).

The role of static pressure fluctuations in the turbulent mechanical energy transfer has been investigated in the scale region where there is an active turbulent shear stress ( $-u'w'$ ). The cospectra of the turbulent kinematic vertical transports of horizontal alongwind momentum and heat are presented in Figure 5. These graphs show that there is a significant transport for scales in the region which includes both regions denoted by 'A' and 'B' in Figure 3.

Also shown in Figure 5 is the cospectrum of the turbulent kinematic vertical static pressure flux. This quantity acts as a source term in both the height-integrated vertical turbulent kinetic energy and the total turbulent kinetic energy budget. For the present, near neutral ASL data ( $z/L \approx -0.01$ , cf Table I), the static pressure-vertical velocity correlation term is small. It amounts to about 3% of the mechanical energy production, by the interaction between the turbulent shear stress and the mean velocity, and is balanced by the upward flux of total turbulent specific kinetic energy. The turbulent vertical flux of static pressure receives its main contribution from the lower end of the

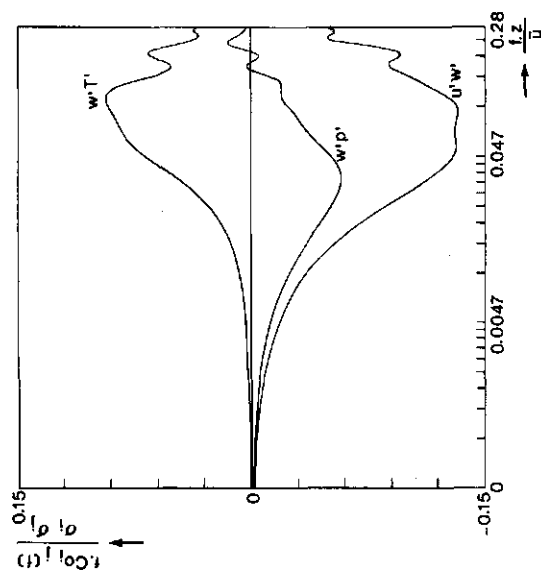


Figure 5 Logarithmic cospectra of turbulent kinematic vertical transports of horizontal alongwind momentum, heat and static pressure, normalized by the variances of the individual turbulent signals.

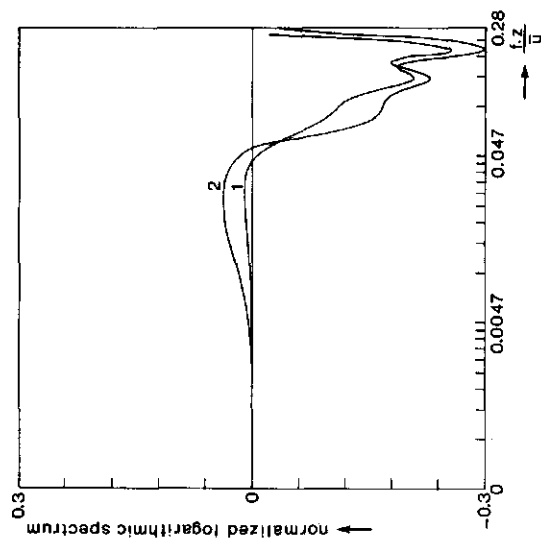


Figure 6 Normalized logarithmic cospectrum between the turbulent static pressure and the differentiated horizontal alongwind velocity fluctuations (1), and the quadrature spectrum between the turbulent static pressure and the horizontal alongwind velocity fluctuations (2). Both graphs represent the spectral distribution of the transfer of turbulent kinetic energy from the horizontal alongwind velocity by static pressure fluctuations.

region in which there is an appreciable turbulent shear stress (cf. Figure 5).

Figure 6 presents the spectral distribution of the transfer of turbulent kinetic energy from the horizontal alongwind velocity component by the static pressure fluctuations, viz.  $p'\partial u'/\partial x$ . This quantity has been calculated in two ways (cf. Elliott, 1972b) as indicated by the two curves in Figure 6. Curve 1 represents the cospectrum between the turbulent static pressure and the differentiated horizontal alongwind velocity fluctuations. The differentiation was performed with respect to the downstream coordinate, using the Taylor hypothesis of frozen turbulence. Curve 2 represents the quadrature spectrum between the turbulent static pressure and the horizontal alongwind velocity fluctuations. The difference between the two curves is a measure of the inaccuracy of the calculations, which amounts to about 10%.

The graphs in Figure 6 indicate that the transfer of turbulent kinetic energy from the horizontal alongwind velocity, by the static pressure fluctuations, dominates at the high frequency end of the region of appreciable turbulent shear stress. The patterns characteristic of the turbulent structures (cf. Figure 4) show that the convergence of the horizontal alongwind velocity fluctuation ( $\partial u'/\partial x = -(1/\bar{U})\partial u'/\partial t < 0$ ) is coincident with a positive static pressure pulse, in a small scale region around the reference-time. The turbulent vertical velocity component gains its maximum energy at these scales (cf. Figure 3).

The quantity  $p'\partial u'/\partial x$ , which is about equal to -15% of the mechanical turbulent energy production, consists of two parts, viz.  $-p'\partial w'/\partial z$  and  $-p'\partial v'/\partial y$ .  $p'\partial w'/\partial z$  goes directly into the vertical velocity fluctuations. The quantity  $p'\partial v'/\partial y$ , which contributes to the horizontal crosswind fluctuations ( $v'$ ), is of minor importance. The turbulent horizontal crosswind velocity gains its maximum energy at larger scales from the horizontal alongwind velocity fluctuations, mainly because of the requirements of continuity.

#### 4. The role of static pressure fluctuations in the mechanism of the origin and development of the turbulent structures

We have a consistent picture of the variation of velocity, static pressure and temperature inside a turbulent structure (cf. Figure 4). The identification of the associated causal relationships will be discussed in this section. Special attention has been paid to the role of the spatial static pressure gradients inside the turbulent structures.

From the phasing relations between the patterns, as shown in Figure 4, it is clear that the ejection ( $w' > 0$ ) of low speed fluid, just before the reference time, occurs during a time when the fluid involved is subjected to a negative streamwise turbulent static pressure gradient ( $\partial p'/\partial x = -(1/\bar{U})\partial p'/\partial t < 0$ ). At the same time, the fluid experiences a strong convergence in the alongwind direction ( $\partial u'/\partial x < 0$ ). The horizontal crosswind velocity component has been shown to be inactive inside an average turbulent structure (Schols, 1984). The vertical velocity must therefore show a strong divergence ( $\partial w'/\partial z > 0$ ) along the upstream interface of the turbulent structure, due to continuity requirements.

This strong vertical stretching along the upstream interface requires an upward directed force working on the fluid in the turbulent structure. The magnitude of this force is determined by the vertical turbulent static pressure gradient and the buoyancy force. For the present, near neutral data, the magnitude of the buoyancy force is about one order of magnitude smaller than the turbulent static pressure gradient force at the observation height of 3.56 m (see appendix E). The vertical turbulent static pressure gradient force at the upstream back of the turbulent structure, which is assumed to be of the same order of magnitude as the streamwise turbulent static pressure gradient force, is sufficiently large to cause the ejection of low-speed fluid.

The vertical gradient of turbulent static pressure provides the

IV.12

link between the small scale and large scale organized motions inside the turbulent structures in the ASL: At the moment that large scale high-speed air masses from higher up are swept to the surface ( $\partial w'/\partial t < 0$ ), the characteristic small scale pulse shape appears in the turbulent static pressure signal. The half part of the pressure pulse, downstream of the internal shear layer, gives rise to a negative spatial turbulent static pressure gradient. The resulting turbulent pressure gradient force causes the ejection of fluid in the turbulent structure.

## 5. Conclusions

The turbulent static pressure fluctuations play a crucial role in the dynamics of turbulent structures in the near neutral ASL. The static pressure variations, as measured in the frequency range between 0.001 and 1 Hz, contain two dominant timescales: An intense, small scale, pulse shaped, fluctuation is imbedded in a large scale variation around the upstream interface of a turbulent structure. The large scale variation is coupled to the passage of convective elements, which contain air lighter than their surroundings. The small scale static pressure pulse is caused by the sharp downward fluctuation of the vertical velocity ( $\partial w'/\partial t < 0$ ), which is associated with the internal shear layer at the upstream back of the turbulent structure.

At the high frequency end of the region of appreciable turbulent shear stress, mechanical turbulent energy is extracted from the horizontal alongwind velocity fluctuations. This energy is mainly fed into the vertical velocity component and takes place through the static pressure-alongwind velocity gradient interactions: The patterns characteristic of the turbulent structures show that the convergence of the horizontal alongwind velocity fluctuations ( $\partial u'/\partial x < 0$ ) coincides with the positive static pressure pulse.

At the low frequency end of the region of active turbulent shear stress, the turbulent static pressure-vertical velocity correlations act as a source term in the height-integrated equation for

the turbulent kinetic energy of the vertical velocity fluctuations. This mechanical energy source term is provided by the negative static pressure fluctuations in relatively light, rising air masses. The term is small in the near neutral ASL, but it becomes increasingly important at greater heights.

The vertical gradient of turbulent static pressure provides the link between the small scale and large scale organized motions inside the turbulent structures in the ASL: The internal shear layer, as determined by the velocity interface, carries a positive static pressure pulse. On the downstream side of the internal shear layer there exists a negative spatial turbulent static pressure gradient which causes the ejection of low speed fluid in the turbulent structures.

## V. Discussion

The planetary boundary layer (PBL) during daytime contains turbulent structures which penetrate into the atmospheric surface layer (ASL), where they modulate the turbulent quantities and show characteristics which are common to turbulent structures in the laboratory shear layer. At the moment when a sharp temperature interface appears, the horizontal alongwind velocity shows a sharp increase, along with a sudden decrease of vertical velocity. This determines a velocity interface or a so-called internal shear layer. The fluctuating static pressure reveals a maximum at this velocity interface at the upstream back of a turbulent structure.

The upstream interface of a turbulent structure is most active. This has also been mentioned by Cantwell (1981) who described the organized motion in laboratory turbulent flows. The magnitude of the vertical turbulent transports is often highest at this interface and it can exceed its long time average value by one order of magnitude.

The turbulence field has a double structure: A sharp small scale fluctuation, at the upstream interface of a turbulent structure, is superimposed on a large scale variation. The interaction process between the large scale motion and the small scale motion can be described in two ways: One is from the viewpoint of static pressure-velocity (gradient) interactions, as has been done in the present study. The other is from the point of view of vorticity. An important role in the development of turbulent structures in the wall region of a laboratory shear layer is credited to the fluctuating small scale vorticity (Willmarth, 1975). It is suggested, in laboratory studies, that the vortex stretching mechanism is a fundamental process in the ejection phase of a turbulent structure.

The mechanism of the origin and development of the turbulent structures in the laboratory shear layer has not yet been re-

solved. This is mainly due to the incompleteness of the measurements of both the small scale turbulent static pressure and vorticity fluctuations. Blake (1970) and Emmerling (1973) definitely determined that measurements of the wall pressure fluctuations are seriously in error with regard to the smallest spatial scales of pressure fluctuations. The error is caused by the inability of the relatively large pressure transducers that are used in experimental work to resolve the smallest spatial scales of the pressure fluctuations. Willmarth (1975) mentioned that it is unfortunate that the proper instrumentation for the measurement of small scale vorticity fluctuations in laboratory turbulent boundary layer flows has not yet been developed.

In the ASL in a turbulent structure, the sweep is on the average preceeded by the ejection. However, their cause and effect relationship indicates that the oncoming high speed velocity interface at the upstream back of a turbulent structure produces an intense small scale static pressure pulse as it travels from greater heights to the surface. In this way, a negative vertical gradient of turbulent static pressure on the downstream side of the velocity interface is produced. The resulting force induces inside the turbulent structure the ejection of low speed fluid.

The Reynolds number in atmospheric turbulent flow, based on the boundary layer thickness, is much larger than in laboratory shear flow. Power spectra in the ASL thus contain more decades than in the laboratory. The laboratory turbulent shear layer contains only two scale regions: A wall region occupies approximately 10% of the total boundary layer thickness and the other region, called the outer region, occupies the remaining part of the boundary layer. The largest turbulence scales and the smallest scales of turbulence are widely separated in the ASL. These two ranges of scales are divided by a third intermediate scale region. This makes the coupling between phenomena appearing in these two extreme scale ranges less clear than in laboratory turbulent shear layers. As an example, it is well established that the mean time between the appearance of turbulent structures in the wall region

of the laboratory shear layer scales with outer region variables. However, in the ASL very little is known about the scaling laws for the spacing of turbulent structures in the alongwind direction.

The present measurement data on the turbulent structures in the ASL need to be completed with similar data from greater heights. Additional knowledge of the behavior of turbulent structures in the region above the ASL can serve as a helpful tool for selecting the scales on which the turbulent structures in the ASL can be normalized to show universal behavior. Webb (1977) stated that the coupling between the turbulent vertical heat transfer in the ASL and above takes place by means of thermal walls. These thermal walls form a distinct and decoupled mechanism from the elongated turbulent structures in the ASL that do not carry up heat out of the ASL. Figure 1, which has been taken from Webb's (1977) paper, shows a schematic picture of convection throughout the whole depth of the PBL. The thermal walls are commonly about 100 m thick and spaced about 3 km (over grassland). They are often arranged in an irregular polygonal pattern. Their height is about 250 to 300 m, and from the thermal wall junctions columnar 'thermals' arise which extend to the top of the PBL and which activate entrainment from the overlying stable air into the PBL. This picture of convection throughout the PBL corresponds with the finding, in appendix B, that, going from the minimum depth, over which convection takes place, to above, the convection mode gradually changes from longitudinal cells to symmetric cells and finally to transverse cells at greater heights.

The present experimental results will be most effective when they are used in model calculations. The development or extension of theoretical models is important, especially for atmospheric research. Essential information on the flow dynamics is lost in generating the classical Reynolds equations through a conventional averaging process. The formulation will have to reflect more explicitly the double-structured nature of the turbulent flow: A time-dependent lower mode (the quasi-ordered large scale struc-

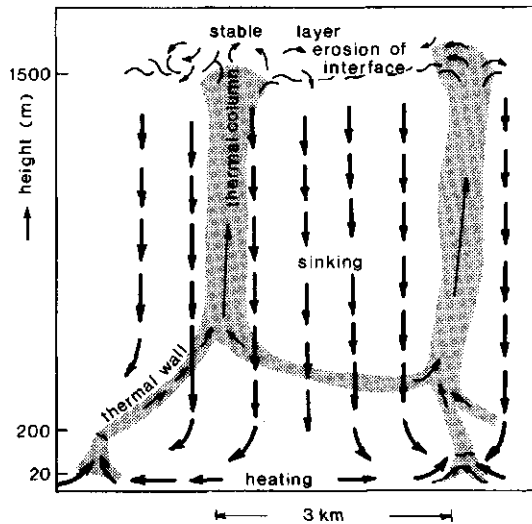


Figure 1. Schematic illustration of thermal structure in the PBL, with typical heights indicated (from Webb, 1977).

ture) interacting with a fine scale randomized motion.

For engineering purposes one is interested in the magnitude of the time-mean turbulent transports, averaged over a certain amount of area. The question is now how to transform point measurements of these turbulent transports to values which are representative of the surface above which they have been obtained. The answer to this question largely depends on how the spatial distribution of the turbulent structures in the ASL is established. On the one hand, a small irregularity on the surface, e.g. a ditch or a fence, can act as a triggering mechanism for the formation of a turbulent structure. In this way, the turbulent structures will, on the average, appear at fixed positions on the surface, which can be located by means of remote sensing techniques. On the

other hand, the turbulent structures are generated as a result of an alteration or disturbance of the flow field caused by the debris produced by an old upstream turbulent structure. This mechanism explains the cyclical occurrence of turbulent structures. Once the spots, where the turbulent structures originate, have been located, point measurements of turbulent quantities can be carried out at these locations. The planform distribution of the turbulent structures, as determined by using IRLS pictures of the surface, can then be used to convert the point measurements into field averaged quantities.

In conclusion, a few final suggestions for future research are given. Artificially generated fixed turbulent structures, by means of line obstacles, can be studied in order to investigate their time-dependent behavior and cyclical distribution. Measurements of the small scale turbulent vorticity during the various stages of development of the turbulent structures is important. Turbulence structure cannot easily be understood without the concept of vorticity.

## Appendix A. Horizontal wind speed averaged over the depth of the ASL

In a near neutral thermally stratified ASL the vertical profile of the mean horizontal alongwind velocity can be described by the logarithmic law

$$\bar{U}/u_* = (1/k) \ln z/z_0, \quad (A.1)$$

where  $k$  denotes the von Kármán constant, which is chosen equal to 0.4.  $u_*$  stands for the surface friction velocity and  $\bar{U}$  is the mean horizontal wind speed at the height  $z$ .  $z_0$  is the surface roughness length, which is equal to 22 mm for the present site.

The magnitude of the mean horizontal wind,  $\bar{U}_{av}$ , averaged over the depth ( $h$ ) of the ASL is obtained by integrating Equation (A.1):

$$\bar{U}_{av}/u_* = \frac{1}{k(h-z_0)} \int_{z_0}^h \ln(z/z_0) dz = \frac{h}{k(h-z_0)} (\ln h/z_0 - 1) \quad (A.2)$$

Under the assumption that  $h$  is of the order of  $1000 z_0$  it follows that

$$\bar{U}_{av} \approx 15u_*$$

$z_0$  and  $u_*$  have been computed using the wind speeds at 2 and 10 m height as provided by the weather station and assuming the logarithmic law.

## Appendix B. Convection cells in the unstable ASL

Kuettner (1971) presents a theory, which shows that the curvature of the vertical velocity profile of a two dimensional flow with no directional change with height enforces alignment of convective cells with the flow direction. Inertial forces arising from the vorticity field counteract buoyancy forces. Their ratio as expressed in a modified Froude number ( $F_m$ ) determines the value of the critical Rayleigh number ( $Ra_c$ ) responsible for the onset of convection. In a flowing medium this critical Rayleigh number is raised, often by several orders of magnitude, over that of a resting medium for all convective modes, except for the longitudinal mode, as is shown in Figure B.1. An application of the simplified theory to ASL conditions is presented below.

The conservation and the vertical transport of differential vorticity by convective motions are important factors in the physical mechanism that determines the convective flow behavior as is shown in Figure B.2. In the ASL the vertical velocity profile is curved and the vorticity,  $\partial \bar{u} / \partial z$ , is decreasing upwards (cf. Figure B.2, left). If a fluid element from a lower level is displaced upwards it conserves its vorticity and constitutes a 'relative vortex' having an excess vorticity over its new environment (cf. Figure B.2, right). The resulting distortion of the basic vorticity field causes fluid elements on the left side of the vortex to be replaced by elements from lower levels (having an excess vorticity) and those on the right side by elements from higher levels (having a vorticity deficiency). This redistribution induces a downward acceleration of the 'vortex' returning the displaced element toward the level where it belonged and where it finds no differential vorticity (Lin, 1955). Fluid elements displaced upwards or downwards under the action of buoyancy forces, inducing an additional vorticity along the direction of the basic non-uniform vorticity field, will therefore have to overcome the restoring forces resulting from the vorticity gradient. Convective motions in a plane along the basic vorticity vector will not meet such restoring forces, since there

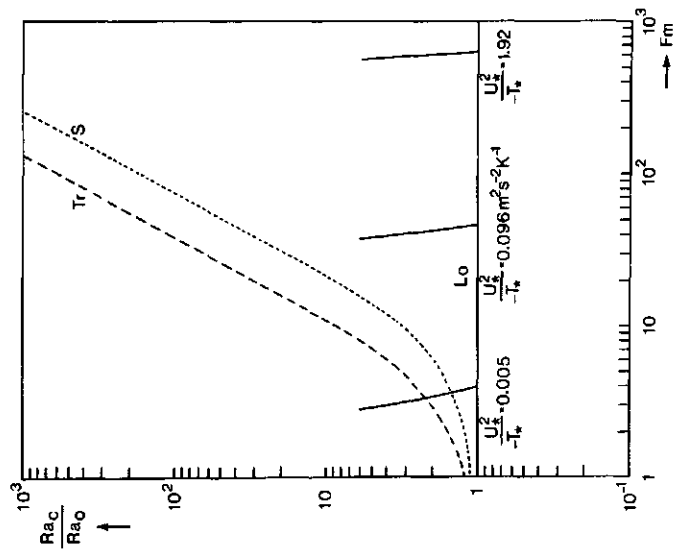


Figure B. 1 Ratio of critical Rayleigh number ( $Ra_c$ ), as defined for transverse bands ( $Tr$ ), symmetric cells ( $S$ ) and longitudinal bands ( $Lo$ ), to its critical value ( $Ra_0$ ) for the case of marginal stability in a medium at rest, as a function of the Froude number ( $Fm$ ) (from Kuettner, 1971).

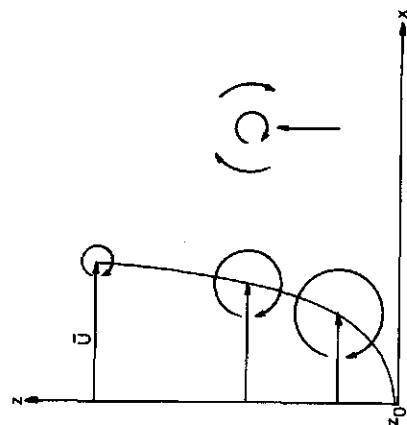


Figure B.2 Schematic presentation of the vertical profile of mean horizontal along-wind velocity in the ASL, its vorticity distribution, and relative vorticity of vertically displaced convective elements (from Kuettner, 1971).

is no basic flow in that plane and thus no differential vorticity vector perpendicular to that plane to inhibit the fluid motion. This mode of convection represents organized helical motions in longitudinal rolls, as is shown in Figure 11.

Kuettner (1971) showed that, under the assumption of a few simplified flow conditions, viz. the Boussinesq approximation and the neglect of the Coriolis force, the convection mode is determined by two dimensionless numbers, viz. the Rayleigh number (Ra) and the Froude number (Fm). The Rayleigh number relates the inertia forces ( $\rho \underline{U} \cdot \nabla \underline{U}$ ) times the buoyancy forces ( $-\rho g \Delta T / \bar{T}$ ) to the square of the viscous forces ( $\rho \nu \nabla^2 \underline{U}$ ). This number is used to characterize the dynamical flow behavior when buoyancy forces are comparable to or dominate over inertia forces. The Froude number relates the square of the vertical shear ( $\partial \bar{U} / \partial z$ ) to the vertical gradient of the buoyancy acceleration ( $(-g / \bar{T}) \partial \bar{T} / \partial z$ ).

In the ASL, assuming the logarithmic law to be valid, the vertical shear is simply connected to the vertical shear gradient ( $\partial^2 \bar{U} / \partial z^2$ ) by means of the equation

$$\frac{\partial \bar{U}}{\partial z} = - z \frac{\partial^2 \bar{U}}{\partial z^2} \quad (B.1)$$

Thus, the Froude number relates the squared vertical shear gradient to the vertical gradient of the buoyancy acceleration, as Kuettner also defined it. The value of the Rayleigh number averaged over a depth h in the ASL is given by

$$Ra_{av} = - (\phi_{m_{av}} \phi_{H_{av}} (g / \bar{T})_{av} T_* / (k^2 u_*^2)) h \quad (B.2)$$

The subscript av refers to averaging over the height h. Using the average values of the dimensionless functions  $\phi_m$  and  $\phi_H$  (Wyngaard and Coté, 1971) and the buoyancy parameter  $(g / \bar{T})$ , Equation (B.2) can be approximated by

$$Ra_{av} = Ah T_* / u_*^2 \quad (B.3)$$

where  $A \approx -0.026 \text{ ms}^{-2}\text{K}^{-1}$ .

The critical Rayleigh number ( $Ra_0$ ) for the onset of convection amounts 6.75. The minimum depth ( $h_{\min}$ ) over which the convection takes place is thus given by

$$h_{\min} = Bu_*^2/T_* \quad , \quad (B.4)$$

where  $B \approx -260 \text{ m}^{-1}\text{s}^2\text{K}$

This height scale determines the diameter of the longitudinal cells, which form the prevailing convection pattern in the ASL (cf. Figure 11). Their lateral wavelength ( $\lambda_y$ ) amounts  $2h_{\min} \sqrt{2}$ .

The average Froude number is written as

$$Fm_{av} = -(\phi_{m_{av}}^2 / (\phi_{H_{av}} (g/\bar{T})_{av} k z_0)) u_*^2 / (T_* \ln(h/z_0)) \quad (B.5)$$

Again using the average values of the dimensionless functions  $\phi_m$  and  $\phi_H$  and the buoyancy parameter this equation can be approximated by

$$Fm_{av} = (Cu_*^2/T_*) / \ln(h/z_0) \quad , \quad (B.6)$$

where  $C \approx -3400 \text{ m}^{-2}\text{s}^2\text{K}$ .

As  $h/z_0$  is of the order of 1000, the average Froude number amounts about  $0.145Cu_*^2/T_*$  and it decreases very little with height.

In Figure B.1 the relationship in the ASL between the Rayleigh number and the Froude number, as obtained by eliminating  $h$  in Equations (B.2) and (B.5), has been drawn for three values of  $u_*^2/T_*$ . The middle curve belongs to the data of Figure 10 and it indicates that the longitudinal mode of convection prevails throughout the entire depth of the ASL. The left curve shows that, going from the minimum depth, over which convection takes

place, to above, the convection mode gradually changes from longitudinal cells to symmetric cells and finally to transverse cells at greater heights.

## Appendix C. Stagnation pressure

The stagnation pressure,  $p_s$ , is defined as:

$$p_s = \frac{1}{2}\rho U^2 \quad , \quad (C.1)$$

where  $\rho$  is the air density and  $U$  stands for the air speed.

The variation of  $p_s$  is given by

$$\Delta p_s = \rho U \Delta U = 2\alpha p_s \quad , \quad (C.2)$$

where  $\alpha = \Delta U/U$ , which amounts to about 0.15 at a turbulence level of 25%. Hence, the variation in the stagnation pressure is about 30% of its magnitude.

As has already been pointed out in appendix A,  $u_* \approx 0.07 \bar{U}_{av}$ .

The root-mean-square static pressure produced by the ASL turbulence at the surface is about 2.6 times the mean turbulent shear stress (Elliott, 1972 b). Thus, the standard deviation of the turbulent static pressure fluctuations amounts to about 3% of the stagnation pressure averaged over the depth of the ASL.

## Appendix D. Turbulent kinetic energy budget

It is assumed that there is a steady state flow ( $\partial \bar{f} / \partial t = 0$ ) and there is homogeneity over all horizontal planes ( $\partial \bar{f} / \partial x = 0$ ). Furthermore, no appreciable influence of the Coriolis forces and effects of evaporation or condensation are considered. Finally, the Boussinesq-approximation is applied.

The budget of turbulent kinetic energy per component is written as (for a description of the symbols see list)

$$\frac{1}{2} \frac{\partial \overline{u'^2}}{\partial t} = 0 = -\frac{1}{2} \frac{\partial}{\partial z} \overline{u'^2 w'} + \frac{1}{\rho} \overline{p' \frac{\partial u'}{\partial x}} - \overline{u' w'} \frac{\partial \bar{U}}{\partial z} - \frac{\bar{\epsilon}}{3} \quad (\text{D.1.1})$$

$$\frac{1}{2} \frac{\partial \overline{v'^2}}{\partial t} = 0 = -\frac{1}{2} \frac{\partial}{\partial z} \overline{v'^2 w'} + \frac{1}{\rho} \overline{p' \frac{\partial v'}{\partial y}} - \frac{\bar{\epsilon}}{3} \quad (\text{D.1.2})$$

$$\frac{1}{2} \frac{\partial \overline{w'^2}}{\partial t} = 0 = -\frac{1}{2} \frac{\partial}{\partial z} \overline{w'^3} + \frac{1}{\rho} \overline{p' \frac{\partial w'}{\partial z}} - \frac{1}{\rho} \frac{\partial}{\partial z} \overline{p' w'} + \frac{g}{T} \overline{w' T'} - \overline{u' w'} \frac{\partial \bar{U}}{\partial z} - \frac{\bar{\epsilon}}{3} \quad (\text{D.1.3})$$

The three equations above, summed together, yield the total turbulent mechanical energy budget equation ( $q'^2 = \frac{1}{2}(\overline{u'^2} + \overline{v'^2} + \overline{w'^2})$ )

$$\frac{\partial \overline{q'^2}}{\partial t} = 0 = -\frac{\partial}{\partial z} \overline{q'^2 w'} - \frac{1}{\rho} \frac{\partial}{\partial z} \overline{p' w'} + \frac{g}{T} \overline{w' T'} - \overline{u' w'} \frac{\partial \bar{U}}{\partial z} - \bar{\epsilon} \quad (\text{D.2})$$

Equation (D.2) is integrated between the surface and height  $z$  (cf. Elliott, 1972b). Under the assumptions of constant mean turbulent shear stress and vertical heat flux, this operation leads to the height-integrated total turbulent kinetic energy equation

$$0 = -\overline{q'^2 w'} - \frac{1}{\rho} \overline{p' w'} + z \frac{g}{T} \overline{w' T'} - \overline{u' w'} \bar{U} - z \bar{\epsilon}_{av} \quad (\text{D.3})$$

Here, it is further assumed that there is negligible turbulent

energy flux through the surface. The subscript av denotes an average value over the height  $z$ .

## Appendix E. Pressure gradient force

The timescales of interest, at the upstream interface of the turbulent structure, lie close to those in the inertial subrange ( $1 < fz/\bar{U} < 10$ ) of turbulence. It is therefore assumed, due to local isotropy considerations, that the vertical gradient of turbulent static pressure is of the same order of magnitude as the downstream turbulent static pressure gradient at the upstream interface of the turbulent structure.

The buoyancy force per mass unit,  $gT'/\bar{T}$ , as determined from the magnitude of the sharp temperature fluctuation at the upstream interface, just before the reference time, amounts to about  $0.004 \text{ ms}^{-2}$ . The downstream gradient of the turbulent static pressure,  $\partial p'/\partial x$ , has been calculated using the Taylor hypothesis of frozen turbulence and assuming a translation speed of the turbulent structure equal to fifteen times the surface friction velocity (Schols et al., 1984). The value of  $\partial p'/\partial x$ , as estimated from the static pressure pattern in Figure 4, is about equal to  $-0.05 \text{ kg m}^{-2} \text{ s}^{-2}$ . The negative vertical gradient of the turbulent kinematic pressure,  $(-1/\rho) \partial p'/\partial z$ , is thus of the order of  $0.04 \text{ ms}^{-2}$ , and yields the largest contribution to the vertical stretching force along the upstream interface of the turbulent structure. This stretching force per unit of mass,  $w' \partial w'/\partial z$ , has been computed using the continuity equation ( $\partial w'/\partial z \approx -\partial u'/\partial x$ ) and the patterns in Figure 4. It has been estimated to be about  $0.02 \text{ m s}^{-2}$ .

## Summary

The turbulent flow in the atmospheric surface layer (ASL) contains turbulent structures, which are defined as spatially coherent, organized flow motions. 'Organized' means that characteristic patterns, observed at a point in space, occur almost simultaneously in more than one turbulence signal and are repeated periodically.

These turbulent structures play an important role in the processes of production and transport of turbulence, and they are central to understanding the mechanism of turbulence. A real life turbulent field is a superposition of effects from numerous structures of varying sizes in different stages of development. Van Atta (1977) suggested that a turbulent flow contains a hierarchy of organized motions in which smaller scale motions are superimposed on larger ones.

The detection of turbulent structures forms a problem with two aspects: First, which flow properties must be used to define a turbulent structure. Second, how can be decided that on the basis of these properties, a turbulent structure is present. The VITA (variable interval time averaging) method concentrates exclusively on the intense, high frequency components of a single turbulent signal at one point in space.

The application of the VITA detection method to ASL turbulence data is described in Chapter II. It works well, since the signal-to-noise ratio is favorable, especially for the temperature fluctuations in the unstable ASL. The qualitative behavior of the conditional averages, using the VITA method, is not sensitive to the selection of the detection parameters, i.e. threshold level and short averaging time. The conditional averages represent ensemble-averaged values of the flow quantities inside the turbulent structures.

The VITA method reveals the presence of vertically coherent tur-

bulent structures in the ASL, which look similar to those in laboratory shear flows. At the moment when a sharp temperature interface appears, the horizontal alongwind velocity shows a sharp increase, along with a sudden decrease of vertical velocity, independent of the thermal stability conditions in the ASL. This determines a velocity interface, which is important in the turbulent transport processes as can be inferred from its relationship to the temperature interface.

The turbulent structures in the ASL produce between 30 and 50 percent of the mean turbulent vertical transport of horizontal alongwind momentum and they contribute to between 40 and 50 percent of the mean turbulent vertical heat transport, both during 15 to 20 percent of the total observation time. Chapter III contains a quantitative description of those turbulent structures, which are most significant for the turbulent transport processes in the ASL. The turbulent structures are the result of the formation of longitudinal convection cells in the unstable ASL. The diameter of these cells scales on the ASL parameters  $u_*$  and  $T_*$ , while the translation speed of the turbulent structures scales on  $u_*$ . Kline et al. (1967) found that the lateral dimensions of the turbulent structures in a laboratory shear layer scaled on the wall region parameters, viz. the wall friction velocity and the molecular kinematic viscosity. Beljaars (1979) presented a deterministic mathematical model for turbulent exchange in a laboratory boundary layer. He introduced counterrotating stream-wise vortices to explain the existence of periodic instability zones in the wall region. These instabilities refer to the burst events, which are part of the turbulent structures. The burst events contain both the ejection and sweep phases of a turbulent structure.

The turbulent structures in the ASL are determined by a large scale temperature field. Convective motions, which encompass the whole depth of the planetary boundary layer (PBL), penetrate into the ASL. The inclination angle of the temperature interface at the upstream edge of the turbulent structures to the surface is

about  $40^\circ$ ; that of the velocity interface, also called internal shear layer, is approximately  $60^\circ$ . The internal shear layer at the back of laboratory shear structures has been found to be inclined at an angle of about  $18^\circ$  to the wall (Thomas and Bull, 1983).

Chapter IV describes the dynamical properties of the turbulent structures in the near neutral ASL. The vertical gradient of turbulent static pressure provides the link between the small scale and large scale organized motions inside the turbulent structures in the ASL: The internal shear layer, as determined by the velocity interface, carries a positive static pressure pulse. On the downstream side of the internal shear layer, at the upstream back of a turbulent structure, there exists a negative spatial turbulent static pressure gradient which causes the ejection of low speed fluid in the turbulent structure.

The turbulent static pressure field contains two dominant time scales: An intense small scale, pulse shaped, fluctuation is imbedded in a large scale variation around the upstream interface of a turbulent structure in the ASL. The large scale pressure field travels at a speed, which is equal to about twice the value of the speed for the small scales. Emmerling's (1973) wall pressure data obtained in a laboratory turbulent shear layer, indicate that intense, individual, small scale pressure fluctuations travel downstream at speeds as low as about half the speed at which the large scale pressure fluctuations move as measured by e.g. Willmarth and Wooldridge (1962). The small scale wall pressure fluctuations are very intense relative to the intensity of the large scale wall pressure fluctuations.

In chapter V the present results are discussed and suggestions for future research are presented.

## Samenvatting

In de oppervlaktegrenslaag van de atmosfeer komen turbulente structuren voor, die gedefinieerd worden als ruimtelijk coherente, georganiseerde stromingspatronen. 'Georganiseerd' wil zeggen dat er, in één punt in de ruimte, in meerdere turbulente signalen, vrijwel gelijktijdig, karakteristieke stromingspatronen voorkomen, die zich periodiek herhalen.

De turbulente structuren spelen een belangrijke rol in de productie en het transport van turbulentie. Verder zijn ze van belang voor een betere begripsvorming van het verschijnsel turbulentie. Een turbulent stromingsveld bestaat uit een superpositie van veel structuren met velerlei afmetingen en in verschillende ontwikkelingsstadia. Van Atta (1977) veronderstelde dat een turbulente stroming uit een hiërarchie van georganiseerde stromingspatronen bestaat, waarin kleinschalige bewegingen zijn gesuperponeerd op bewegingen met een grotere schaal.

De detectie van turbulente structuren vormt een tweeledig probleem: 1. Welke eigenschappen van de stroming moeten worden gebruikt om een turbulente structuur te definiëren. 2. Hoe kan, op basis van deze eigenschappen, worden beslist of er een turbulente structuur voorkomt. De VITA (variabele interval time averaging) methode benadrukt de intensieve, hoog frequente componenten van een turbulent signaal.

De toepassing van de VITA detectiemethode op de turbulente signalen in de atmosferische oppervlaktegrenslaag wordt beschreven in hoofdstuk II. De methode voldoet goed, omdat de signaal-ruisverhouding gunstig is, in het bijzonder voor de temperatuurfluctuaties in een thermisch onstabiel gelaagde oppervlaktegrenslaag. Het kwalitatieve gedrag van de conditionele gemiddelden is ongevoelig voor de keuze van de parameters van de VITA methode, t.w. drempelwaarde en korte middelingstijd. Conditionele gemiddelden stellen ensemble-gemiddelden voor van de stromingsvariabelen

binnen de turbulente structuren.

De VITA methode brengt de aanwezigheid van verticaal coherente turbulente structuren in de oppervlaktegrenslaag aan het licht. Deze turbulente structuren vertonen gelijkenis met die in laboratoriumgrenslagen. Op het moment dat er een scherp temperatuurgrensvlak aanwezig is, vertoont de horizontale component van de snelheid in de richting van de gemiddelde wind een sterke toename, terwijl de verticale component van de windsnelheid een plotselinge daling vertoont. Dit gedrag van beide snelheidscomponenten is onafhankelijk van de thermische gelaagdheid in de oppervlaktegrenslaag. Hierdoor wordt een snelheidsgrensvlak bepaald, dat van belang is voor de turbulente transportprocessen, hetgeen volgt uit de relatie met het temperatuurgrensvlak.

De turbulente structuren in de oppervlaktegrenslaag produceren tussen 30 en 50 procent van het gemiddelde turbulente verticale transport van de horizontale component van impuls in de gemiddelde windrichting, en ze dragen tot tussen 40 en 50 procent van het gemiddelde turbulente verticale warmtetransport bij. Beide bijdragen vinden plaats binnen 15 tot 20 procent van de totale observatieduur. Hoofdstuk III bevat een kwantitatieve beschrijving van de turbulente structuren die het belangrijkste zijn voor de turbulente transportprocessen in de oppervlaktegrenslaag. De turbulente structuren zijn het gevolg van longitudinale convectiecellen in de thermisch onstabiel gelaagde oppervlaktegrenslaag. De diameter van deze cellen schaaft op de parameters  $u_*$  en  $T_*$  van de oppervlaktegrenslaag. De voortplantingssnelheid van de turbulente structuren schaaft op  $u_*$ . Kline e.a. (1967) vonden dat de zijdelingse afmetingen van de turbulente structuren in een laboratoriumgrenslaag schaalden op de wandparameters, namelijk de wrijvingssnelheid en de kinematische moleculaire viscositeit. Beljaars (1979) presenteerde een wiskundig model voor het turbulente transport in een laboratoriumgrenslaag. Hij introduceerde tegen elkaar indraaiende wervels in de langsrichting om het voorkomen van periodieke instabiliteitszones in het wandgebied te verklaren. Deze instabiliteiten zijn burst-gebeurtenis-

sen, die een onderdeel vormen van de turbulente structuren. De burst-gebeurtenissen omvatten zowel de uitstoot- als de instuif-fase van een turbulente structuur.

De turbulente structuren in de oppervlaktegrenslaag worden door een grootschalig temperatuurveld bepaald. Convectieve bewegingen, die zich over de gehele hoogte van de atmosferische grenslaag voordoen, dringen tot in de oppervlaktegrenslaag door. De hellingshoek van het temperatuurgrensvlak, aan de achterzijde van de turbulente structuren, met het aardoppervlak is ongeveer  $40^\circ$ ; die van het snelheidsgrensvlak, ook interne schuifspanningslaag geheten, is ongeveer  $60^\circ$ . De interne schuifspanningslaag aan de achterzijde van turbulente structuren in een laboratoriumgrenslaag maakt een hoek van ongeveer  $18^\circ$  met de wand (Thomas en Bull, 1983).

In hoofdstuk IV worden de dynamische eigenschappen van de turbulente structuren in een bijna neutrale oppervlaktegrenslaag beschreven. De verticale gradiënt van de turbulente statische druk vormt de verbinding tussen de kleinschalige en grootschalige georganiseerde bewegingen binnen de turbulente structuren in de oppervlaktegrenslaag: De interne schuifspanningslaag, bepaald door het snelheidsgrensvlak, bevat een positieve puls in de statische druk. Aan de stroomafwaartse zijde van de interne schuifspanningslaag, aan de stroomopwaartse achterzijde van een turbulente structuur, bestaat een negatieve ruimtelijke turbulente statische drukgradiënt. Deze drukgradiënt veroorzaakt de uitstoot van fluïdum met geringe snelheid in de turbulente structuur.

Het turbulente statische drukveld bevat twee dominante tijdschalen: Een heftige kleinschalige, pulsvormige, fluctuatie is ingebed in een grootschalige variatie rond het stroomopwaartse grensvlak van een turbulente structuur in de oppervlaktegrenslaag. Het grootschalige drukveld beweegt zich met een snelheid, die ongeveer gelijk is aan twee maal de waarde van de snelheid van de kleinere schalen. De resultaten van Emmerling (1973), uit

een turbulente laboratoriumgrenslaag, tonen aan dat intensieve, individuele, kleinschalige drukfluctuaties zich stroomafwaarts verplaatsen met snelheden die ongeveer de helft bedragen van de snelheid waarmee de grootschalige drukfluctuaties bewegen, zoals door bijvoorbeeld Willmarth en Wooldridge (1962) is gemeten. De kleinschalige drukfluctuaties aan de wand zijn zeer heftig in vergelijking met de intensiteit van de grootschalige drukfluctuaties aan de wand.

In hoofdstuk V worden de huidige resultaten ter discussie gesteld en worden suggesties voor verder onderzoek gedaan.

## References

- Antonia, R.A., Chambers, A.J., Friehe, C.A. and Van Atta, C.W.: 1979, 'Temperature ramps in the atmospheric surface layer', *J. Atmos. Sci.* **36**, 99-108.
- Beljaars, A.C.M.: 1979, 'A model for turbulent exchange in boundary layers', Ph. D. thesis, Eindhoven Univ. of Techn.
- Blackwelder, R.F. and Kaplan, R.E.: 1976 'On the wall structure of the turbulent boundary layer', *J. Fluid Mech.* **76**, 89-112.
- Blake, W.K.: 1970, 'Turbulent boundary layer wall pressure fluctuations on smooth and rough walls', *J. Fluid Mech.* **44**, 637-660.
- Businger, J.A., Miyake, M., Dyer, A.J. and Bradley, E.F.: 1967, 'On the direct determination of the turbulent heat flux near the ground', *J. Appl. Meteorol.* **6**, 1025-1032.
- Cantwell, B.J.: 1981, 'Organized motion in turbulent flow', *Ann. Rev. Fluid Mech.* **13**, 457-515.
- Chen, C.-H.P. and Blackwelder, R.F.: 1978, 'Large-scale motion in a turbulent boundary layer: A study using temperature contamination', *J. Fluid Mech.* **89**, 1-31.
- Derksen, W.J.: 1974, 'Thermal infrared pictures and the mapping of micro-climate', *Neth. J. Agric. Sci.* **22**, 119-132.
- Driedonks, A.G.M., Dop, H. van, and Kohsiek, W.H.: 1978, 'Meteorological observations on the 213 m mast at Cabauw in the Netherlands', 4th Symp. Met. Obs. Instr., Denver, Colorado.
- Driedonks, A.G.M., Nieuwendijk, P.A.T. and Goes, C.J.: 1980, 'A set of computer programs to process turbulence data, measured at the 200 m mast at Cabauw', *Sci. Rep. W.R.* 80-3 K.N.M.I.
- Driedonks, A.G.M.: 1981, 'Dynamics of the well-mixed atmospheric boundary layer', *Sci. Rep. W.R.* 81-2 K.N.M.I.
- Elliott, J.A.: 1972a, 'Instrumentation for measuring static pressure fluctuations within the atmospheric boundary layer', *Boundary-Layer Meteorol.* **2**, 476-495.

- Elliott, J.A.: 1972b, 'Microscale pressure fluctuations measured within the lower atmospheric boundary layer', J. Fluid Mech. 53 , 351-383.
- Emmerling, R.: 1973, 'The instantaneous structure of the wall pressure under a turbulent boundary layer flow', Max-Planck-Institut für Strömungsforschung, Bericht no. 9.
- Haugen, D.A., Kaimal, J.C. and Bradley, E.F.: 1971, 'An experimental study of Reynolds stress and heat flux in the atmospheric surface layer', Quart. J. Roy. Meteorol. Soc. 97 , 168-180.
- Johansson, A.V. and Alfredsson, P.H.: 1982, 'On the structure of turbulent channel flow', J. Fluid Mech. 122 , 295-314.
- Kaimal, J.C. and Businger, J.A.: 1970, 'Case studies of a convective plume and a dust devil', J. Appl. Meteorol. 9 , 612-620.
- Kaimal, J.C.: 1974, 'Translation speed of convective plumes in the atmospheric surface layer', Quart. J. Roy. Meteorol. Soc. 100 , 46-52.
- Kaimal, J.C., Wyngaard, J.C., Haugen, D.A., Coté, O.R., Izumi, Y., Caughey, S.J. and Readings, C.J.: 1976, 'Turbulence structure in the convective boundary layer', J. Atmos. Sci. 33 , 2152-2169.
- Kaplan, R.E. and Laufer, J.: 1968, 'The intermittent turbulent region of the boundary layer', Univ. South. Calif. Rep. USCAE 110.
- Khalsa, S.J.S.: 1980, 'The limitations of stress-parameterization imposed by intermittency in turbulent flow', Boundary-Layer Meteorol. 19 , 3-17.
- Kim, H.T., Kline, S.J. and Reynolds, W.C.: 1971, 'The production of turbulence near a smooth wall in a turbulent boundary layer', J. Fluid Mech. 50 , 133-160.
- Kline, S.J., Reynolds, W.C., Schraub, F.A. and Runstadler, P.W.: 1967, 'The structure of turbulent boundary layers', J. Fluid Mech. 30 , 741-773.
- Kuettner, J.P.: 1971, 'Cloud bands in the earth's atmosphere. Observations and theory', Tellus 23 , 404-426.

- Lenschow, D.H. and Stephens, P.L.: 1980, 'The role of thermals in the convective boundary layer', *Boundary-Layer Meteorol.* 19, 509-532.
- Lin, C.: 1955, 'The theory of hydrodynamic stability', Cambridge University Press, 155 pp.
- Phong-Anant, D., Antonia, R.A., Chambers, A.J. and Rajagopalan, S.: 1980, 'Features of the organized motion in the atmospheric surface layer', *J. Geophys. Res.* 85, 424-432.
- Priestley, C.H.B.: 1959, 'Turbulent transfer in the lower atmosphere', University of Chicago Press, Chicago.
- Reynolds, O.: 1895, 'On the dynamical theory of incompressible viscous fluids and the determination of the criterion', *Phil. Trans. Roy. Soc. London* 186, 123-164.
- Schols, J.L.J.: 1984, 'The detection and measurement of turbulent structures in the atmospheric surface layer', *Boundary-Layer Meteorol.* 29, 39-58, Chapter II of this dissertation.
- Schols, J.L.J., Jansen, A.E. and Krom, J.G.: 1984, 'Characteristics of turbulent structures in the unstable atmospheric surface layer', (submitted to *Boundary-Layer Meteorol.*), Chapter III of this dissertation.
- Subramanian, C.S., Rajagopalan, S., Antonia, R.A. and Chambers, A.J.: 1982, 'Comparison of conditional sampling and averaging techniques in a turbulent boundary layer', *J. Fluid Mech.* 123, 335-362.
- Taylor, R.J.: 1958, 'Thermal structures in the lowest layers of the atmosphere', *Austr. J. Phys.* 11, 168-176.
- Tennekes, H.: 1970 'Free convection in the turbulent Ekman layer of the atmosphere', *J. Atmos. Sci.* 27, 1027-1034.
- Tennekes, H.: 1973, 'A model for the dynamics of the inversion above a convective boundary layer', *J. Atmos. Sci.* 30, 558-567.
- Thomas, A.S.W. and Bull, M.K.: 1983, 'On the role of wall-pressure fluctuations in deterministic motions in the turbulent boundary layer', *J. Fluid Mech.* 128, 283-332.
- Van Atta, C.W.: 1977, 'Effect of coherent structures on structure functions of temperature in the atmospheric boundary layer', *Archives of Mech.* 29, 161-171.

- Van Maanen, H.R.E. and Fortuin, J.M.H.: 1983, 'Experimental determination of the random lump-age distribution in the boundary layer of the turbulent pipe flow using laser-doppler anemometry', Chem. Engineering Sci. 38 , 399-423.
- Webb, E.K.: 1977, 'Convection mechanisms of atmospheric heat transfer from surface to global scales', Proc. Sec. Austr. Conf. on Heat and Mass Transfer, 523-539, Univ. of Sydney.
- Wilczak, J.M. and Tillman, J.E.: 1980 'The three-dimensional structure of convection in the atmospheric surface layer', J. Atmos. Sci. 37 , 2424-2443.
- Willmarth, W.W. and Wooldridge, C.E.: 1962, 'Measurements of the fluctuating pressure at the wall beneath a thick turbulent boundary layer', J. Fluid Mech. 14 , 187-210.
- Willmarth, W.W.: 1975, 'Structure of turbulence in boundary layers', Adv. in Appl. Mech. 15 , 159-254.
- Wyngaard, J.C. and Coté, O.R.: 1971, 'The budgets of turbulent kinetic energy and temperature variance in the atmospheric surface layer', J. Atmos. Sci. 28 , 190-201.
- Zangvil, A.: 1981, 'Some aspects on the interpretation of spectra in meteorology. Boundary-Layer Meteorol. 21 , 39-45.

## Curriculum vitae

Jacobus Leonardus Josephus Schols werd geboren op 13 december 1953 te Neerbeek.

In 1972 behaalde hij het eindexamen Atheneum-B aan de Scholengemeenschap St. Michiel te Geleen.

Daarna werd begonnen met de studie technische natuurkunde aan de Technische Hogeschool te Eindhoven. Het afstudeeronderzoek werd verricht bij de vakgroep Transportfysica (prof. dr. D.A. de Vries) met als onderwerp "The response of a turbulent boundary layer to a step change in surface roughness" (mentoren: prof. dr. K. Krishna Prasad en drs. A.M. Koppius). Het diploma natuurkundig ingenieur werd behaald in juni 1979, waarbij tevens de onderwijsbevoegdheid in de natuurkunde en de mechanica werd verkregen.

Hierna volgde de militaire dienst, die werd vervuld in de functie van reserve-officier bij het Prins Maurits Laboratorium te Rijswijk (Z. H.).

Eind 1980 startte het promotie-onderzoek aan de Landbouwhogeschool te Wageningen bij de vakgroep Natuur- en Weerkunde binnen de sectie Meteorologie.

